Research article

JHEP|Reports

Selective disruption of NRF2-KEAP1 interaction leads to NASH resolution and reduction of liver fibrosis in mice

Authors

Klaus Seedorf, Csaba Weber, Cedric Vinson, Sylvie Berger, Laurent-Michel Vuillard, Arpad Kiss, Stephanie Creusot, Olivier Broux, Anne Geant, Catherine Ilic, Karine Lemaitre, Johann Richard, Adel Hammoutene, Julien Mahieux, Virginie Martigny, Didier Durand, Fabien Melchiore, Miklos Nyerges, Valerie Paradis, Nicolas Provost, Valérie Duvivier, Philippe Delerive

Correspondence

philippe.delerive@nestle.com (P. Delerive).

Graphical abstract

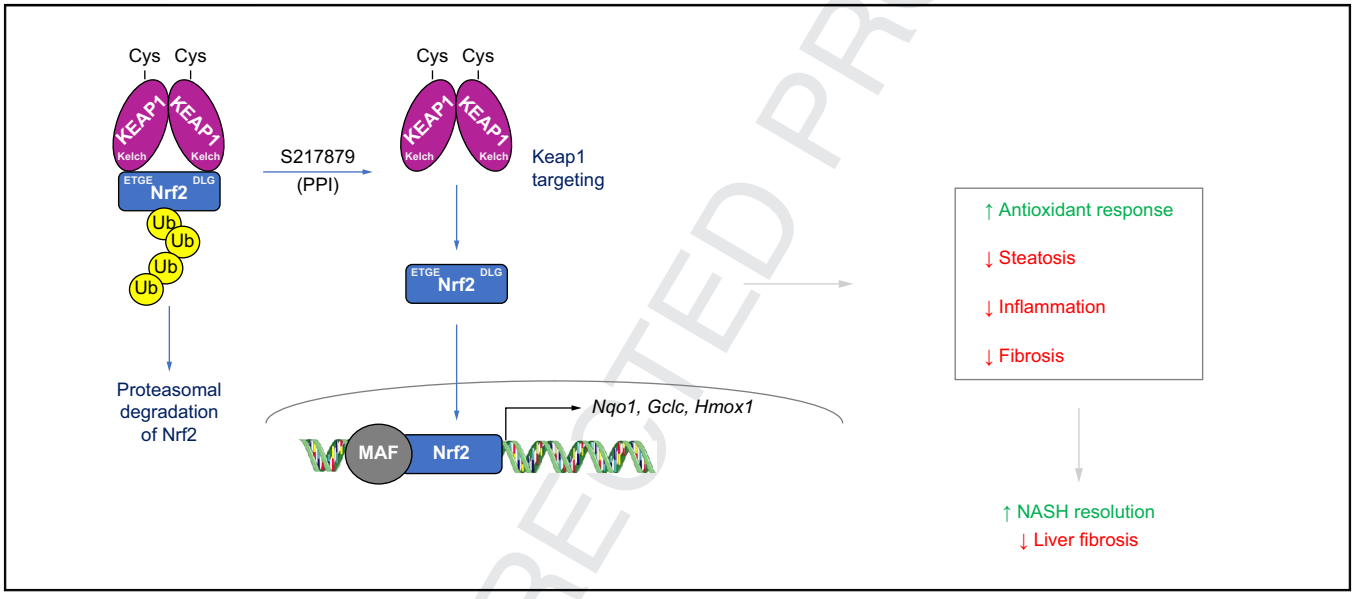

Highlights

- S217879 is a potent and selective compound that disrupts the KEAP1-NRF2 interaction leading to robust NRF2 pathway activation.
- S217879 treatment prevents NASH progression in mice fed a methionine- and choline-deficient diet.
- S217879 treatment significantly reduces both NAS score and fibrosis in DIO-NASH mice.
- NRF2 activation triggers upregulation of the anti-oxidant response and coordinated regulation of a wide spectrum of genes.

https://doi.org/10.1016/j.jhepr.2022.100651

FLA 5.6.0 DTD ■ JHEPR100651_grabs ■ 28 January 2023 ■ 2:10 pm ■ ce

Research article

JHEP|Reports

Selective disruption of NRF2-KEAP1 interaction leads to NASH resolution and reduction of liver fibrosis in mice

Klaus Seedorf,[1,†] **Csaba Weber**,[2,†] Cedric Vinson,[4] Sylvie Berger,[3] Laurent-Michel Vuillard,[3] Arpad Kiss,[2] Stephanie Creusot,[1] Olivier Broux,[1] Anne Geant,[1] Catherine Ilic,[1] Karine Lemaitre,[1] Johann Richard,[3] Adel Hammoutene,[1,5] Julien Mahieux,[4] Virginie Martiny,[3] Didier Durand,[3] Fabien Melchiore,[3] Miklos Nyerges,[2] Valerie Paradis,[6] Nicolas Provost,[1] Valérie Duvivier,[1] Philippe Delerive[1,*]

[1]Cardiovascular and Metabolic Diseases Research, Institut de Recherches Servier, Suresnes, France; [2]Servier Research Institute of Medicinal Chemistry, Záhony u. 7., H-1031 Budapest, Hungary; [3]Institut de Recherche Servier, 125 Chemin de Ronde, 78290 Croissy-sur-Seine, France; [4]Technologie Servier, 27 Rue Eugène Vignat, 45000 Orleans, France; [5]Université Paris Cité, Inserm, Centre de recherche sur l'inflammation, F-75018 Paris, France; [6]Département de Pathologie, Hôpital Beaujon, Assistance Publique-Hôpitaux de Paris, Clichy, France

JHEP Reports **2023.** https://doi.org/10.1016/j.jhepr.2022.100651

Background & Aims: Oxidative stress is recognized as a major driver of non-alcoholic steatohepatitis (NASH) progression. The transcription factor NRF2 and its negative regulator KEAP1 are master regulators of redox, metabolic and protein homeostasis, as well as detoxification, and thus appear to be attractive targets for the treatment of NASH.
Methods: Molecular modeling and X-ray crystallography were used to design S217879 – a small molecule that could disrupt the KEAP1-NRF2 interaction. S217879 was highly characterized using various molecular and cellular assays. It was then evaluated in two different NASH-relevant preclinical models, namely the methionine and choline-deficient diet (MCDD) and diet-induced obesity NASH (DIO NASH) models.
Results: Molecular and cell-based assays confirmed that S217879 is a highly potent and selective NRF2 activator with marked anti-inflammatory properties, as shown in primary human peripheral blood mononuclear cells. In MCDD mice, S217879 treatment for 2 weeks led to a dose-dependent reduction in NAFLD activity score while significantly increasing liver *Nqo1* mRNA levels, a specific NRF2 target engagement biomarker. In DIO NASH mice, S217879 treatment resulted in a significant improvement of established liver injury, with a clear reduction in both NAS and liver fibrosis. αSMA and Col1A1 staining, as well as quantification of liver hydroxyproline levels, confirmed the reduction in liver fibrosis in response to S217879. RNA-sequencing analyses revealed major alterations in the liver transcriptome in response to S217879, with activation of NRF2-dependent gene transcription and marked inhibition of key signaling pathways that drive disease progression.
Conclusions: These results highlight the potential of selective disruption of the NRF2-KEAP1 interaction for the treatment of NASH and liver fibrosis.
Impact and implications: We report the discovery of S217879 – a potent and selective NRF2 activator with good pharmacokinetic properties. By disrupting the KEAP1-NRF2 interaction, S217879 triggers the upregulation of the antioxidant response and the coordinated regulation of a wide spectrum of genes involved in NASH disease progression, leading ultimately to the reduction of both NASH and liver fibrosis progression in mice.

Introduction

Non-alcoholic fatty liver disease (NAFLD) is a common and progressive disease mainly characterized by hepatic fat accumulation in the absence of alcohol consumption. NAFLD is strongly associated with obesity, metabolic syndrome, type 2 diabetes and dyslipidemia. NAFLD is subdivided into non-alcoholic fatty liver (NAFL) and non-alcoholic steatohepatitis (NASH) based on histological examination of liver biopsy and defined by the presence of inflammation and hepatocyte ballooning with various degrees of fibrosis.[1,2] NAFLD is the most common cause of chronic liver disease worldwide, with an estimated prevalence of 25%. It is therefore considered as a global health problem associated with a significant socioeconomic burden.[3,4] In contrast to NAFL, which is considered as a benign and reversible disease state, NASH accounts for an increased number of patients with cirrhosis, liver failure and hepatocellular carcinoma.[5] NAFLD further increases the risk of mortality in a population with a high cardiovascular risk. Long-term follow-up studies revealed that fibrosis is the main driver of mortality in NASH.[6,7] NAFLD remains an unmet medical need since there are no approved therapies despite significant R&D efforts (See[8] for review). NAFLD disease phenotype results from the chronic exposure to environmental factors on a susceptible polygenic background comprising multiple independent modifiers.[9]

Keywords: NASH; fibrosis; NRF2; oxidative stress.
Received 1 June 2022; received in revised form 25 November 2022; accepted 7 December 2022; available online 16 December 2022
† Both authors contributed equally to this work
* Corresponding author. Address: Cardiovascular and Metabolic Diseases Research, Institut de Recherches Servier, Suresnes, France
E-mail address: philippe.delerive@nestle.com (P. Delerive).

Several genes have been associated with the development of NAFLD and more generally liver diseases using genome-wide association studies (see[10] for review). From a mechanistic standpoint, it is believed that the accumulation of both triglycerides and proinflammatory and cytotoxic lipid oxidation side-products results in the formation of a necro-inflammatory milieu which triggers the activation of the main fibrogenic hepatic cell population, namely hepatic stellate cells. Oxidative stress is largely recognized as a major driver of NASH progression.[11] Patients with NAFLD usually display increased levels of lipid peroxidation products and systemic oxidative stress markers.[12,13] Furthermore, histological analyses confirmed that patients with NAFLD exhibit a significant increase in 4-hydroxynonenal-positive cells in the liver.[14,15] 4-hydroxynonenals are formed during lipid peroxidation of polyunsaturated fatty acids. Finally, there is a marked decrease of glutathione and hepatic antioxidant enzymes in patients with NAFLD.[16] Indeed, the insulin resistance-mediated increase in oxidative phosphorylation is a major source of oxidative stress which triggers hepatocellular damage and further exacerbates insulin resistance. Satapati and colleagues have shown that hepatic oxidative stress and inflammation are associated with an elevated oxidative metabolism of saturated fatty acids in NAFLD.[17] Adaptation of mitochondrial function during NAFL is lost in NASH, with increased reactive oxygen species (ROS), lipid peroxidation products and decreased ATP content leading to necrosis and fueling the development of steatohepatitis.[18] Since oxidative stress plays a major role in NASH disease progression, as well as the development of liver fibrosis,[11,19] it is an attractive target for the treatment of NASH.

The nuclear factor erythroid 2–related factor 2 (NRF2), a member of the cap' n' collar basic leucine zipper transcription factor family, and its negative regulator, the E3 ligase adaptor Kelch-like ECH associated protein 1 (KEAP1), are master regulators of cellular resistance to oxidants (See Dodson *et al.* for review[20]). Under resting conditions, NRF2 is sequestered within the cytoplasm. The N-terminal domain of the KEAP1 homodimer binds one molecule of NRF2 leading to ubiquitination by the E3 ligase complex, namely CUL3/RBX1 and ultimately to proteasomal degradation.[21,22] Under oxidative conditions, increased levels of electrophilic molecules result in the covalent modifications of highly reactive cysteine residues within KEAP1 triggering conformational changes and the release of CUL3.[23–26] NRF2 is then released and translocates into the nucleus where it accumulates and dimerizes with small MAF proteins to activate transcription of genes containing the so-called antioxidant response element (ARE).[27,28] NRF2 regulates the transcription of more than 250 genes bearing an ARE involved in antioxidant cellular defense, xenobiotic metabolism and detoxification, carbohydrate and lipid metabolism, protein degradation as well as inflammation.[29] It is therefore not surprising that the NRF2 signaling pathway is considered as a valid target for a number of acute and chronic diseases for which oxidative stress and inflammation are key biological drivers.[30] Increased oxidative stress is a hallmark of chronic liver diseases which explains why NRF2 biology has been extensively probed in the liver (See[31] for review 2014). Interestingly, Nrf2-deficient mice display an increased susceptibility to the development of NASH and fibrosis when placed on a high-fat diet for 24 weeks.[32] Biochemical and molecular analyses revealed that NRF2 protects against NASH, at least in part, by regulating oxidative stress and suppressing *de novo* lipogenesis, endoplasmic reticulum stress and inflammation.[32] Similar findings, namely marked increases in steatosis, inflammation and oxidative stress have been reported in *Nrf2* knockout mice fed a methionine- and choline-deficient diet (MCDD).[33,34] Conversely, sustained NRF2 activation in *Keap1* gene knockdown mice prevented MCDD-induced liver injury.[35] Furthermore, NRF2 pharmacological activation of using potent electrophilic compounds such as 1-[2-cyano3-,12-dioxooleana-1,9(11)-dien-28-oyl] imidazole (CDDO-Im), TBE-31, sulforaphane and omaveloxolone were shown to limit NASH progression and fibrosis in multiple preclinical models.[35–38] Finally, NRF2 protein levels have been shown to be significantly reduced in livers from obese patients with NASH but not NAFL.[39,40] Taken together, all these studies strongly support NRF2 targeting for the treatment of NASH and liver fibrosis. While a number of electrophilic NRF2 agonists delivered initially promising results for various therapeutic indications in preclinical models, they all suffer from a reduced safety margin, mainly due to their limited selectivity and pleiotropic pharmacology, preventing their clinical evaluation in randomized trials for NASH. Bardoxolone has been shown to interact with more than 500 molecular species[41] and to inhibit the endothelin-1 signaling pathway and increase cardiovascular risk in patients with chronic kidney disease.[42,43] The availability of KEAP1 X-ray structure[44] opened the door to the discovery of second-generation NRF2 activators with a completely different way of engaging the target via the direct disruption of its interaction with KEAP1.[45] This led to the identification of potent and selective compounds but with limited oral bioavailability.[46] Herein, we report the discovery and characterization of S217879, a potent and selective small molecule disrupting the KEAP1-NRF2 interaction with good pharmacokinetic properties upon oral administration in rodents. Then, we evaluated its potential as a novel treatment for NASH and liver fibrosis in two different preclinical models.

Materials and methods

S217879

S217879 was synthesized by Servier medicinal chemistry department and was determined to be >98% pure by high-performance liquid chromatography and/or nuclear magnetic resonance analysis (chemical synthesis described within the supplementary information).

LPS-induced cytokine secretion assay

Human peripheral blood mononuclear cells (hPBMCs) were provided by Lonza (#CC-2702). hPBMCs (150,000 cells/well) were plated in 96 well plates in RPMI1640 medium supplemented with 10% FCS, 2% Glutamax and 2% penicillin-streptomycin cocktail (Life Technologies). Cells were then pre-incubated at 37 °C for 4 h with various concentrations of S217879 or vehicle (DMSO, 0.1%). hPBMCs were then stimulated with lipopolysaccharide (LPS: 10 ng/ml) for 4 h. At the end of the stimulation period, cytokine secretion was evaluated using MagPix multiplex kits (Biorad) according to manufacturer's instructions.

Animals

Mice were maintained on a 12:12 h light/dark cycle at 21 ± 2 °C and had *ad libitum* access to tap water and standard (A04) or MCD or AMLN diets. All procedures were performed according to the ethical protocol that has been approved by the Servier Institutional Animal Care and Use Committee in accordance with the French regulations (Decree n° 2013-118 from 01 February

2013 relative to the protection of animals used for scientific purposes and 4 for orders).

MCDD models

8-week-old male C57BL6/J mice (Janvier labs, France) were randomly assigned to either control diet (A04 diet, SAFE) or the MCDD (BROGAARDEN, open source diets) for 2 weeks. Mice on MCDD immediately received either S217879 (3 or 30 mg/kg/day) or vehicle (hydroxyethyl cellulose [HEC] 1%) by gavage for 2 weeks. At the end of the study, mice were fasted for 4 h before termination. Intracardiac blood samples were collected on anesthetized animals (using isoflurane). Liver samples were collected for biochemical, histological and gene expression analyses.

DIO NASH model

5–6-week-old C57BL/6JRj mice were fed with an AMLN diet (D09100301, Research Diet, US) (40% fat [18% trans-fat], 40% carbohydrate [20% fructose], and 2% cholesterol) for 33 weeks prior to initiation of the treatment protocol. Prior to treatment, all mice underwent liver biopsy for confirmation and stratification of liver steatosis and fibrosis, using the NAFLD activity score (NAS) and fibrosis staging system as previously described.[47] Only mice with fibrosis stage ≥1 and steatosis score ≥2, were included in the study. DIO NASH mice were kept on an AMLN diet and received either S217879 (30 mg/kg, PO, QD) or vehicle (HEC 1%) for 8 weeks. A terminal blood sample was collected from the tail vein in non-fasted mice and used for plasma biochemistry. Animals were sacrificed by cardiac puncture under isoflurane anesthesia. Liver samples were processed as described below.

Histological analyses

Formalin-fixed, paraffin-embedded livers were sliced into 3 μm sections. H&E staining was performed to investigate liver histology and Picrosirius red (PSR) staining was used for liver fibrosis. Type 1 collagen (Southern Biotech, #1310-01), galectin-3 and alpha smooth muscle actin (αSMA, Abcam, Ab124964) immunohistochemistry were performed using standard procedures. NAS and fibrosis stage were determined by two double-blinded persons using the NASH Clinical Research Network scoring system.[48] For hepatocellular steatosis, livers were classified into scores 0 to 3 (0: <5% of hepatocytes presenting steatosis, 1: 5 to 33% of hepatocytes presenting steatosis, 2: 33 to 66% of hepatocytes presenting steatosis and 3: >66% of hepatocytes presenting steatosis). For inflammation, livers were scored into grades 0 to 3 (0: non-inflammatory foci, 1: 1 inflammatory focus, 2: 2 to 4 inflammatory foci, 3: >4 inflammatory foci). Fibrosis was scored into stages from 0 to 4 (0: no fibrosis, 1: perisinusoidal or periportal fibrosis, 2: perisinusoidal and periportal fibrosis, 3: bridging fibrosis or septa, 4: cirrhosis).

Biochemical analyses

Plasma parameters were determined with an automatic biochemical analyzer (Indiko Clinical Chemistry Analyzer, Thermofisher). Liver triglyceride levels were measured using a commercially available kit (Roche Diagnostics) after homogenization and extraction as described.[49] For hydroxyproline levels, liver samples are homogenized in 6 M HCl and hydrolyzed to degrade collagen. Samples are centrifuged and the hydroxyproline content is measured in duplicates in the supernatant, using a colorimetric assay (Quickzyme Biosciences) according to the manufacturer's instructions.

Gene expression studies by reverse-transcription quantitative PCR

Total RNA was extracted using Qiagen RNeasy Lipid extraction kit following manufacturer's instructions. Total RNA was treated with DNase I (Qiagen) at 37 °C for 30 min, followed by inactivation at 75 °C for 5 min. Reverse-transcription quantitative PCR assays were performed using an Applied Biosystems QuantStudio 7 Flex System. Total RNA (1 μg) was reverse transcribed with random hexamers using Hight-Capacity cDNA Reverse Transcription Kit with RNase Inhibitor (Applied Biosystems, ThermoFisher Scientific) following the manufacturer's protocol. Gene expression levels were determined with the Taqman Universal Master mix (2x) using Taqman assays (Applied Biosystems). The 18S transcript was used as an internal control to normalize the variations for RNA amounts. Gene expression levels are expressed relative to 18S mRNA levels. All primers used in this study were provided by Thermofisher.

Liver RNA-sequencing

Total RNA was extracted using Qiagen RNA extraction kits following manufacturer's instructions. RNA concentrations were obtained using nanodrop or a fluorometric Qubit RNA assay (Life Technologies, Grand Island, New York, USA). The quality of the RNA (RNA integrity number) was determined on the Agilent 2100 Bioanalyzer (Agilent Technologies, Palo Alto, CA, USA) as per the manufacturer's instructions. To construct the libraries, 400 ng of high-quality total RNA sample (RNA integrity number >8) was processed using TruSeq Stranded mRNA kit (Illumina) according to the manufacturer's instructions. Briefly, after purification of poly-A-containing mRNA molecules, mRNA molecules are fragmented and reverse transcribed using random primers. Replacement of dTTP with dUTP during the second strand synthesis will enable the achievement of strand specificity. Addition of a single A base to the cDNA is followed by ligation of Illumina adapters. Libraries were quantified by qPCR using the KAPA Library Quantification Kit for Illumina Libraries (KapaBiosystems, Wilmington, MA) and library profiles were assessed using the DNA High Sensitivity LabChip kit on an Agilent Bioanalyzer. Libraries were sequenced on an Illumina NovaSeq 6000 instrument using 150 base-lengths read V2 chemistry in a paired-end mode. Sequence reads were trimmed to remove possible adapter sequences and nucleotides with poor quality using Trimmomatic v.0.36. The trimmed reads were mapped to the *Mus musculus* GRCm38 reference genome available on ENSEMBL using the STAR aligner v.2.5.2b. Unique gene hit counts were calculated by using the featureCounts from the Subread package v.1.5.2. Only unique reads that fell within exon regions were counted. Counts have been normalized in transcripts per million using the standard formula.

RNA-seq data analyses

Data analyses were carried out using R system software (http://www.R-project.org, V4.0.2) packages including those of Bioconductor or original R code. Gene hit counts were used for downstream differential expression analysis. Using DESeq2, a comparison of gene expression between the S217879-treated samples and vehicle samples was performed. The Wald test was used to generate p values and $\log_2$ fold changes. Genes with an adjusted p value <0.05 and absolute $\log_2$ fold-change >1 (fold-change >2) were considered as differentially expressed genes between conditions. Enrichment analysis was performed by applying the fast gene set-enrichment analysis (fgsea function

from fgsea R package v.1.16.0, pre-ranked mode) against two separated genesets collections, HALLMARK and a combination of KEGG- and Reactome-curated pathways. Representations of data and results have been generated with ComplexHeatmap v.2.6.2 and ggplot2 v.3.3.5 packages. Data are available under the GSE212644 accession number.

Statistical analysis

For comparison of two groups, an unpaired Student's *t* test was used (GraphPad Prism software) after verification of the normal distribution of data. For more than two groups, a one-way ANOVA was performed followed by a Dunnett's multiple comparison test. For body weight, a two-way ANOVA was performed followed by a Tukey's test. For histological parameters, a statistical model ANOVA was performed with strain and diet as fixed effects on a score parameter (NAS, steatosis, fibrosis or inflammation), followed by least-square mean estimations (SAS software). Significance threshold was 5%. Results are expressed as mean ± SEM.

Results

Non-covalent inhibitors of the KEAP1 Kelch/NRF2 protein-protein interaction may increase selectivity with reduced cytotoxicity, translating into a larger therapeutic index. Several groups have reported the discovery of such molecules. Most of them exhibit promising binding affinities. However, they usually suffer from poor ADME-pharmacokinetic properties limiting their use for probing NRF2 biology *in vivo*. Davies and colleagues reported the discovery of KI-696 (1) (Fig. 1), a potent compound which activates the NRF2 antioxidant response in cellular models. *In vivo* target engagement required i.v. infusion due to its poor oral bioavailability.[46] KI-696 binding to the Kelch domain has been confirmed by X-ray crystallography.[50] More recently, the discovery of a novel non-covalent chemotype with an acceptable pharmacokinetic profile for oral dosing was reported.[51] Preliminary *in vivo* results of the best compound (2) (Fig. 1) revealed target engagement as measured by NRF2-driven gene induction from 10 mg/kg onwards.[51] The X-ray structure of compound 1 and compound 2 Kelch complexes revealed the possibility of macrocyclization which is generally known to modify the entropic contribution to binding.[52] In addition, variation of the linker's position and substitution allows for the fine-tuning of the physicochemical properties without disrupting the interactions with the protein. We decided to replace the benzoxathiazepine and benzoyl scaffolds of 1 and 2 with benzoxathiazine in the hope that the binding mode would exhibit the same key interactions as the parent molecules, with improved

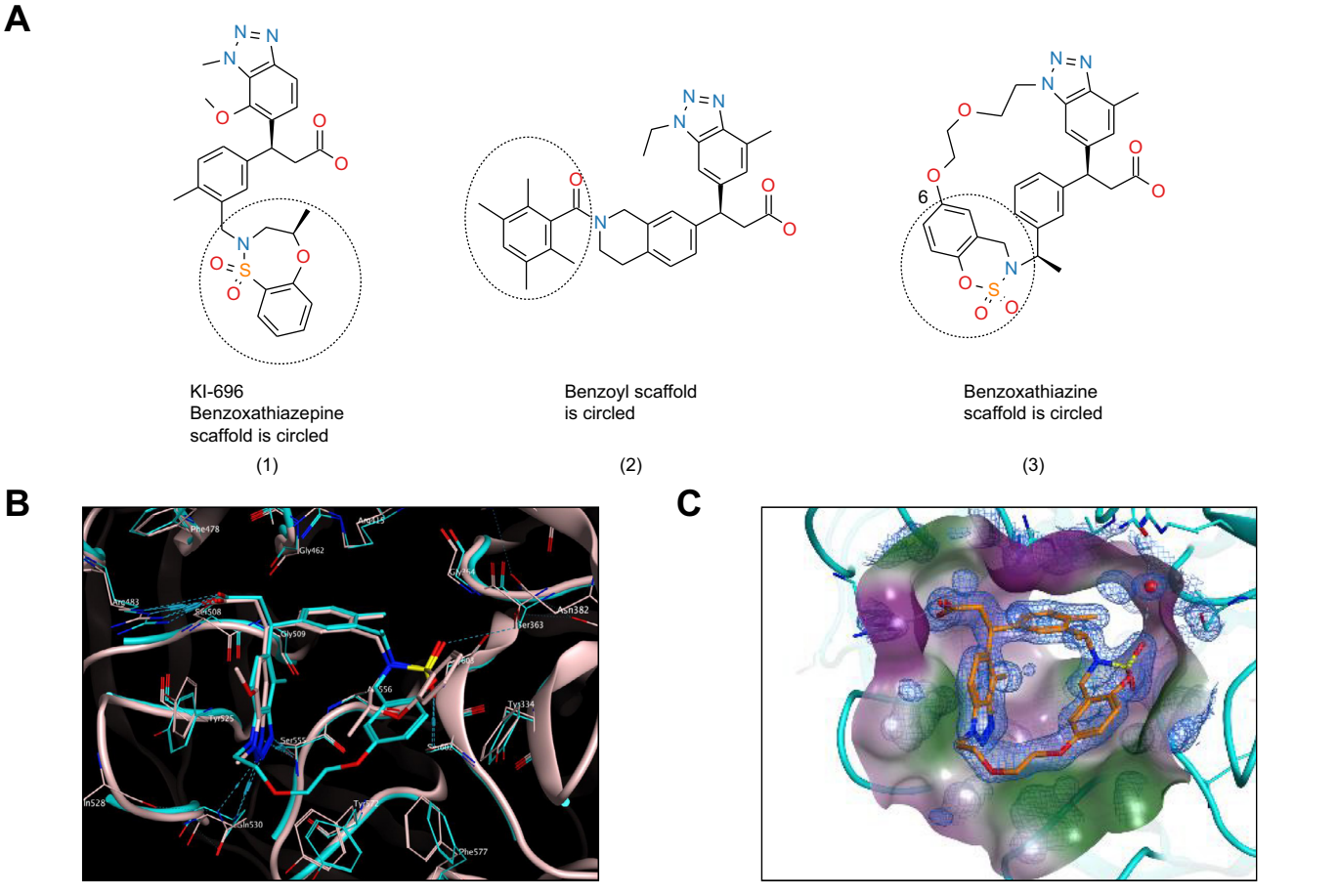

Fig. 1. Identification of S217879 as a novel NRF2 activator. (A) Chemical structure of Kelch-NRF2 interaction disruptors: (1) PPI compound with *in vivo* target engagement established upon i.v. infusion[46] (2) PPI compound with *in vivo* target engagement established upon oral administration[51] (3) Chemical structure of novel PPI compound with good developability profile aka S217879. (B) Overlay of X-ray structures 5GNU (compound 1, grey) and compound 3 (cyan). (C) Crystal structure of the Kelch domain of KEAP1 bound to S217879 (resolution: 1.3 Angström). PPI, protein-protein interaction.

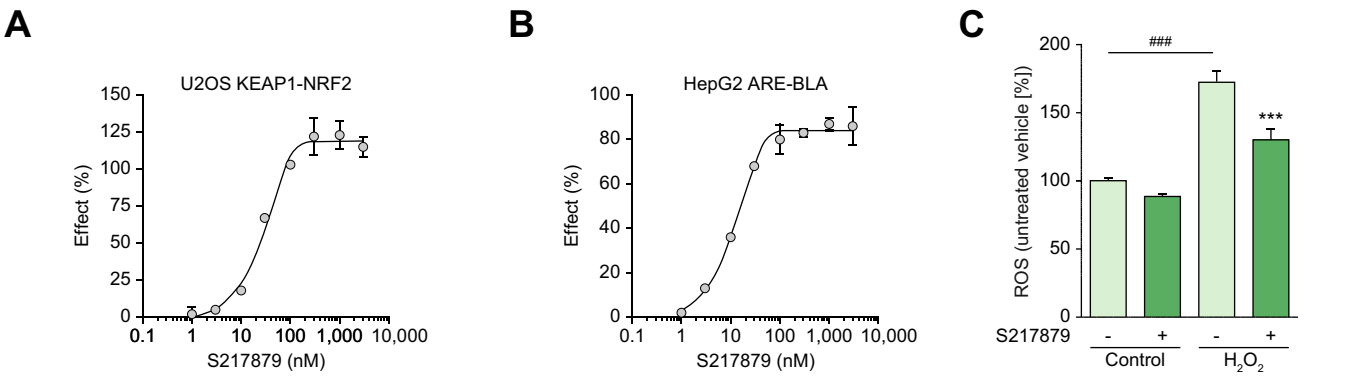

Fig. 2. S217879 is a potent NRF2 activator in cell-based assays. (A) S217879 triggers NRF2 translocation in U2OS cells in a concentration-dependent manner (2 experiments performed in triplicates; data expressed as mean ± SEM). (B) Activation of ARE-driven transcription in HepG2 cells in response to S217879 (2 experiments performed in triplicates; data expressed as mean ± SEM). (C) S217879 pretreatment (1 mM overnight, DMSO 0.1% used as vehicle) limits H_2O_2-triggered ROS generation in HepG2 cells (n = 5 per condition, data expressed as mean ± SEM). Statistical significance was assessed by one-way ANOVA followed by Dunnett's multiple comparison test. $^{###}p$ <0.001 H_2O_2-triggered *vs.* untriggered cells, $^{***}p$ <0.001 S217879-treated *vs.* vehicle.

hydrophobic interactions (Tyr334, Phe557). We hypothesized that position 6 of the benzoxathiazine's benzene ring would provide a suitable vector for linking the aromatic ring with benztriazole's N-alkyl group and would tolerate diverse substitution patterns on the linker. Substutition of the benzyl position next to the benzoxathiazine nitrogene atom also proved to be an effective tool to fine-tune the interaction between benzoxathiazine oxygenes and the protein. Optimization of the macrocyclics' structure was focused on the linker part and led to the synthesis and subsequent selection of compound 3 (See 0;

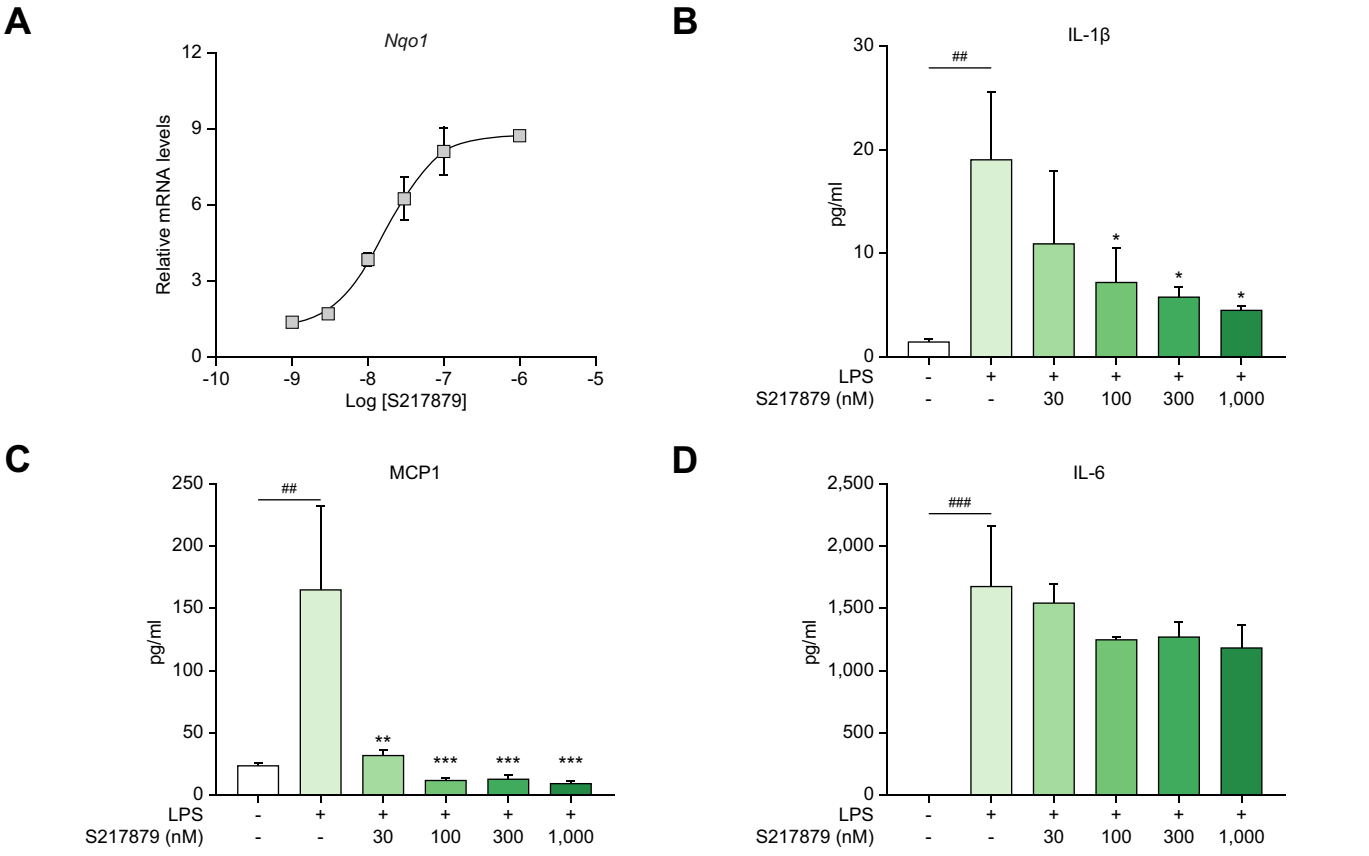

Fig. 3. Inhibition of LPS-driven inflammatory response by S217879 in PBMCs. (A) *Nqo1* gene upregulation in human PBMCs in response to increasing concentrations of S217879 (6 h incubation; DMSO 0.1% used as vehicle). (B-D) Inhibition of LPS-stimulated cytokine secretion in human PBMCs exposed to increasing concentrations of S217879 (4 h pre-incubation; DMSO 0.1% used as vehicle). Data expressed as mean ± SEM. Statistical significance was assessed by one-way ANOVA followed by Dunnett's multiple comparison test. $^{##}p$ <0.01 and $^{###}p$ <0.001: LPS-triggered *vs.* untriggered cells. $^{*}p$ <0.05, $^{**}p$ <0.01 and $^{***}p$ <0.001: S2178789-treated *vs.* vehicle.

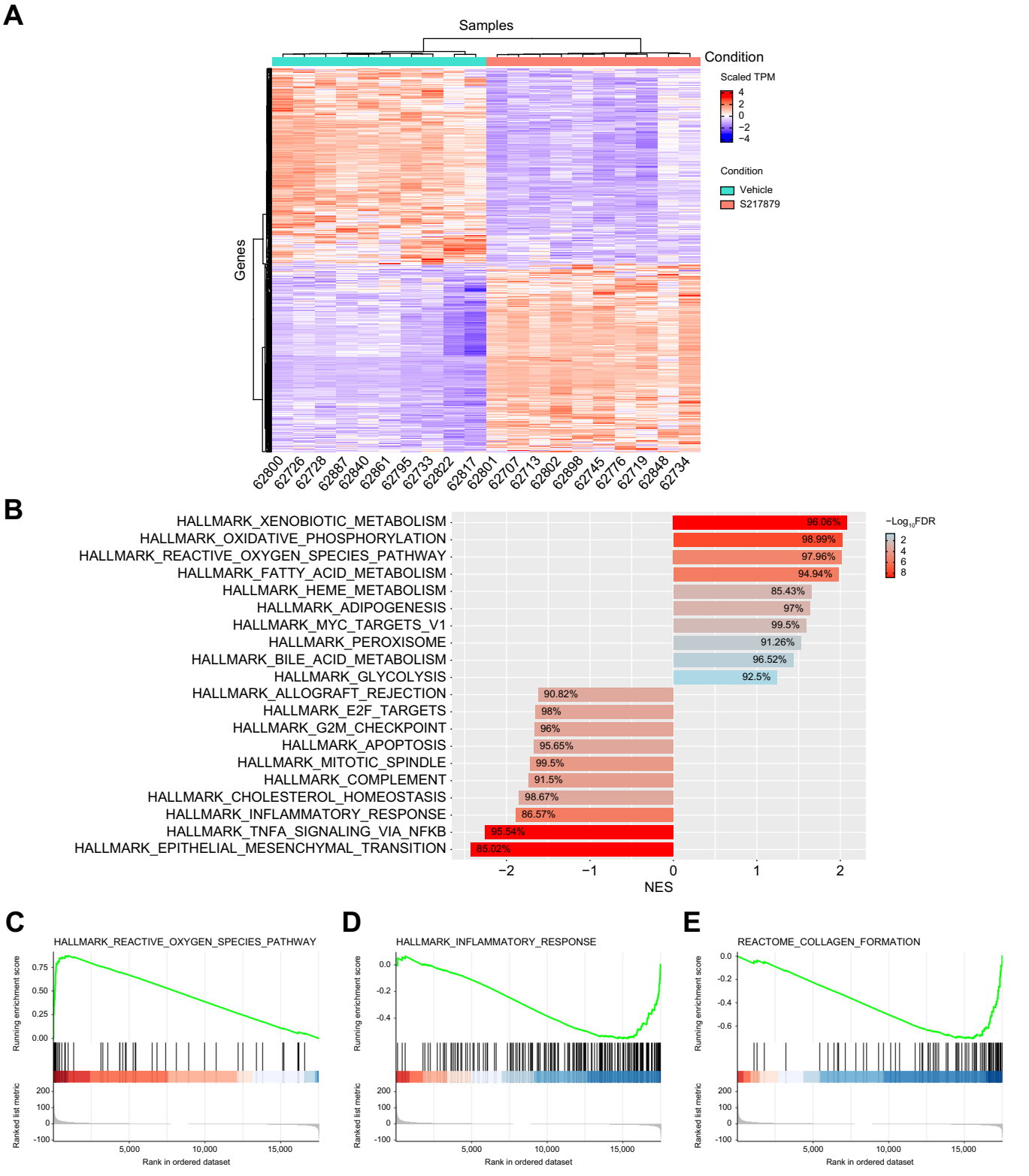

Fig. 7. S217879-mediated NRF2 activation leads to upregulation of the antioxidant response and suppression of a wide spectrum of genes involved in disease progression. (A) Heatmap of differentially expressed genes from S217879-treated DIO NASH mice *vs.* vehicle (Log_2 fold-change cut-off >1; FDR-adjusted *p* value cut-off: 0.05). (B) Gene set-enrichment analysis of differentially expressed genes from DIO NASH mice treated with S217879 or vehicle (HEC 1%). Enriched pathways from gene ontology analysis. (C-E) Gene sets from Hallmark and Reactome revealed upregulated and downregulated pathways (enrichment plots). (C) Reactive oxygen species, (D) inflammatory response and (E) collagen formation. NES, normalized enrichment score.

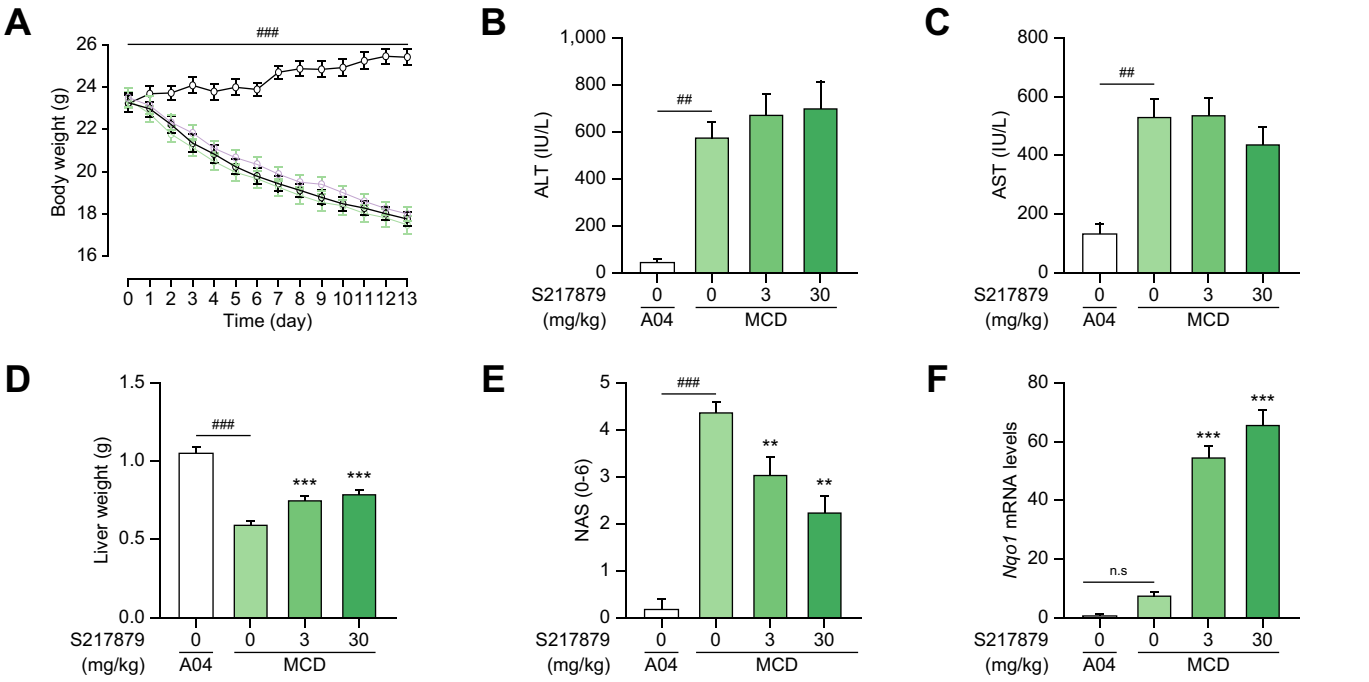

Fig. 4. S217879 reduced NASH progression in MCDD mice in a dose-dependent manner. (A) Body weight evolution throughout the study. (B) Plasma ALT levels at termination. (C) Plasma AST levels at termination. (D) Liver weight at termination. (E) NAFLD activity scores. (F) Liver *Nqo1* mRNA levels expressed as fold induction over control (A04-fed group). Data expressed as mean ± SEM (n = 15 per group). Statistical significance was assessed by one-way ANOVA on log-transformed data followed by a Holm's adjustment for the comparisons of each dose of S217879 *vs.* MCDD vehicle group. $^{\#\#}p$ <0.01, $^{\#\#\#}p$ <0.001: MCD *vs.* A04 (control diet). $^{***}p$ <0.001, $^{**}p$ <0.01 S217879-treated *vs.* vehicle. n.s., non-significant.

Compound 3 is referred to as S217879 throughout the manuscript) as a candidate. Binding to KEAP1 Kelch domain was confirmed with a direct surface plasmon resonance assay (Kd = 4.15 nM; Table S1). The X-ray cocrystal structure confirmed that the benzoxathiazine ring's position allowed for improved interactions with hydrophobic residues (Tyr334, Phe557, Fig. 1C). Then, we assessed the ability of S217879 to trigger NRF2 nuclear translocation in U2OS cells using a beta galactosidase complementation assay. Andrographolide, a plant-derived diterpenoid was used at 10 μM as a positive control. Andrographolide triggers NRF2 nuclear translocation by forming adducts with cysteine 151 within KEAP1.[53] S217879 induced a concentration-dependent increase in NRF2 translocation in U2OS cells with an EC_{50} of 23 nM (Fig. 2A). In line with these results, S217879 significantly activated a reporter gene driven by an ARE in HepG2 cells in a concentration-dependent manner with an EC_{50} of 18 nM (Fig. 2B). Since NRF2 is a master regulator of cellular resistance to oxidants (See Dodson *et al.* for review[0]), we next tested S217879's ability to reduce H_2O_2-stimulated ROS production in HepG2 cells. As expected, H_2O_2 triggered a significant increase in ROS production which was significantly reduced by S217879 treatment (Fig. 2C). Taken together, these results indicate that S217879 is a potent NRF2 activator *in vitro*.

Next, S217879 was evaluated in a broad selectivity panel comprising 110 targets. In this panel, S217879 was tested at 10 μM, a roughly 2,000-fold higher concentration with respect to KEAP1 binding. Interestingly, none of these targets were significantly activated or inhibited in response to S217879, strongly supporting its selectivity (Table S2).

Since NRF2 activation has been shown to inhibit LPS-driven inflammation independently of redox control in both monocytes and macrophages,[54] we next evaluated the anti-inflammatory properties of S217879 in primary hPBMCs. In hPBMCs, S217879 treatment for 6 h resulted in a concentration-dependent increase in *Nqo1* gene expression with an EC_{50} of 16 nM (Fig. 3A) in line with its cell-based potency determined in both HepG2 and U2OS cells (Fig. 2). As expected, LPS triggered a robust and significant increase in IL-1β, IL-6 and MCP-1 secretion (Fig. 3B-D). Pretreatment for 4 h with S217879 led to a significant and concentration-dependent inhibition of LPS-induced cytokine release as measured by IL1β, MCP-1 and IL6 MagPix multiplex assays (Fig. 3B-D). Of note, both IL-1β and MCP-1 secretion were significantly reduced by S217879 treatment (IC_{50} <30 nM in line with NRF2 cell-based potency) in contrast to IL-6 which was slightly and not significantly reduced at higher concentrations (Fig. 3B-D). NRF2 has been shown to negatively interfere with the NF-κB pathway which regulates the expression of a wide spectrum of inflammatory genes.[54] Why IL6 regulation seems to be less sensitive to NRF2 remains unknown. Nevertheless, these data indicate that S217879 displays significant anti-inflammatory properties in hPBMCs (Fig. 3B-D) while strongly engaging the NRF2 signaling pathway (Fig. 3A).

In vitro ADME and safety parameters were profiled comprehensively to identify an orally available and safe compound (Table S3). The ability of S217879 to activate the NRF2 signaling pathway *in vivo* was next evaluated in C57BL6 mice. Male C57BL6 mice received a single administration of S217879 (30 mg/kg) or vehicle (HEC 1%) by gavage. Drug plasma exposure was quantified over time and NRF2 target engagement was assessed in the liver by measuring *Nqo1* mRNA levels by reverse-transcription quantitative PCR. S217879 drug levels rise rapidly following oral administration with Cmax reaching 3.2 μM (Fig. S1). Plasma concentrations declined rapidly (AUC = 3.8 μM h) while *Nqo1*

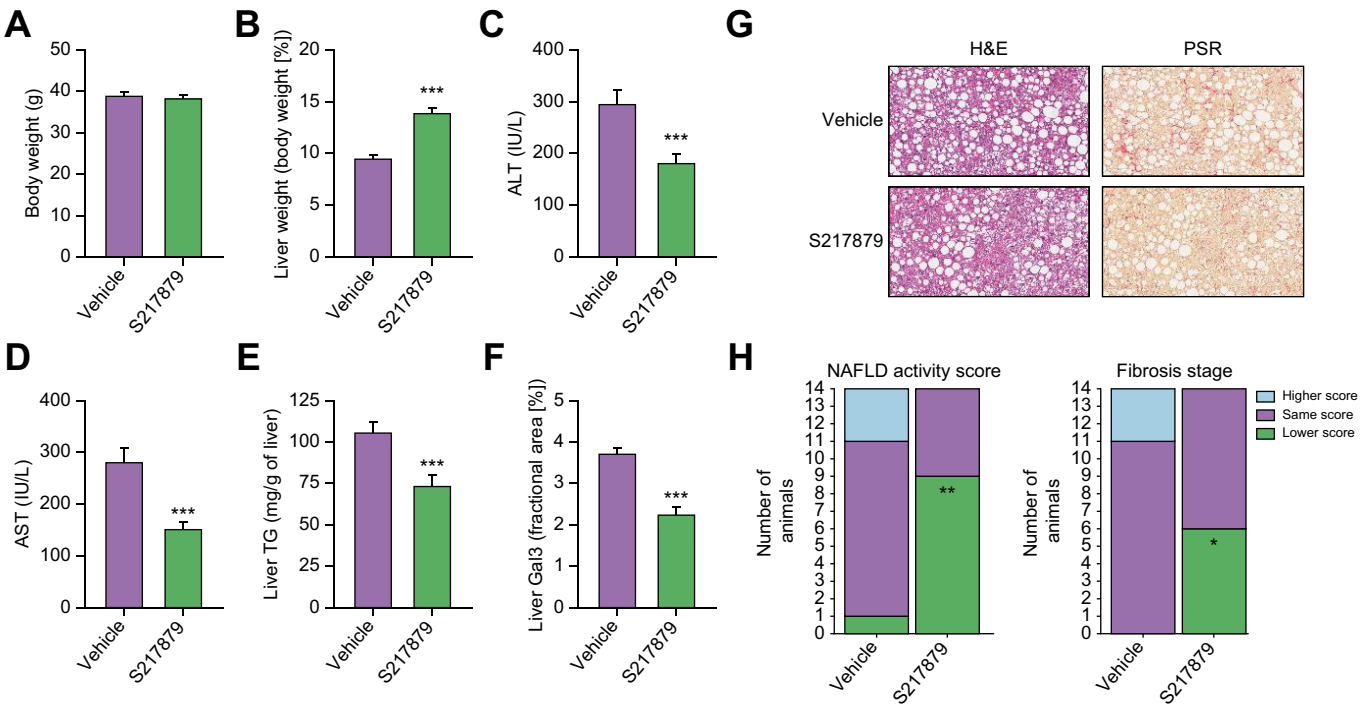

Fig. 5. S217879 reduced NASH progression and liver fibrosis in DIO NASH mice model. (A) Body weight at the end of the study. (B) Liver weight expressed as percentage of total body weight. (C) Plasma ALT levels. (D) Plasma AST levels. (E) Liver TGs. (F) Liver Gal3-positive area. Data expressed as mean ± SEM (n = 14 per group). (G) H&E and PSR-stained liver sections. (H) Summary of histopathological NAFLD activity (left graph) scoring and fibrosis stage (left graph) of pre- and post-study biopsies. For each group, the number of animals with a higher (worsening), same or lower (improvement) score at post- compared to pre-study is indicated by the height of the bar. (A-F) Significant differences were analyzed using Student's *t* test. (H) Significance of number of animals with a lower score *vs.* vehicle was assessed using Fisher's exact test followed by correction for multiple comparisons using the Bonferroni method. ***p <0.001, **p <0.01 and *p <0.05: S217879-treated *vs.* vehicle.

mRNA levels in the liver increased in a time-dependent manner, reaching an up to 10-fold increase over vehicle 24 h post oral administration (Fig. S1A). Similar results were obtained in the kidney (data not shown). Of note, S217879 treatment (single or chronic administration) was found to increase the hepatic expression of numerous NRF2 target genes such as *Gclc, Gstm1, Gpx2* (Fig. S1B, Fig. 7, Figs. S7–8). These results indicate that S217879 oral administration leads to NRF2 pathway activation *in vivo*.

Having characterized S217879 as a potent and selective NRF2 activator *in vitro* and *in vivo*, we next evaluated its potential for the treatment of NASH using two well-established preclinical models. First, the MCDD mouse model was selected as a screening model to test the ability of S217879 to prevent or limit disease progression. This model is highly reproducible and mice rapidly develop a NASH-like liver phenotype after just a few weeks (see[55] for review). Furthermore, this model was initially used to genetically validate NRF2 as a potential target for NASH.[33–35] As expected, mice fed the MCDD rapidly lost weight compared to mice receiving the control diet (Fig. 4A). Two weeks of exposure to MCDD led to significant liver injury with a sharp increase in plasma liver enzymes (Fig. 4B-C). Histological analyses confirmed the development of NASH with severe steatosis and hepatic inflammation reaching a NAS >4 (Fig. 4E, Table S5) in line with previous reports.[56] While treatment with S217879 at 3 and 30 mg/kg/day had no effect on total body weight *vs.* vehicle (Fig. 4A), it significantly improved liver histology with a dose-dependent reduction in NAS (Fig. 4E, Fig. S2). A reduction in both steatosis and lobular inflammation scores was recorded at the highest dose (Table S5). Interestingly, this reduction in NAS was not followed by a reduction of plasma liver enzymes (Fig. 4B,C). These data are consistent with previous results obtained by Okada and colleagues who reported an impact of constitutive NRF2 activation on liver enzymes only after 13 weeks on MCDD.[34] Biochemical analyses confirmed a dose-dependent reduction in liver triglycerides in response to S217879 treatment in MCDD-fed mice (Fig. S3) in agreement with our histological analyses (Fig. 4E, Table S5). As expected, the S217879-mediated reduction in NAS occurred at doses which triggered significant NRF2 target engagement as measured by the dose-dependent increase in liver *Nqo1* mRNA levels (Fig. 4F, Fig. S4) in line with the dose-dependent increase in drug exposure (Table S3). It is noteworthy that the MCDD itself triggered the upregulation of antioxidant response as shown previously.[57] Gene expression studies confirmed the clear upregulation of the antioxidant response in response to S217879 with significant *Gpx2* gene induction (Fig. S4). In addition, S217879 treatment led to significant inhibition of the expression of proinflammatory genes such as *Ccl5, Cd68, Il1b* and *Il6* (Fig. S4). These results are consistent with the anti-inflammatory properties of S217879 described in hPBMCs (Fig. 3). Finally, analyses of genes involved in *de novo* lipogenesis such as *Fasn, Acaca* and *Scd1* revealed a lack of effect of S217879 on their expression levels (Fig. S4). Sugimoto and colleagues failed to demonstrate a major impact of NRF2 activation on fatty acid metabolism genes in MCDD-fed mice.[34] Notably, we observed a small but significant increase in liver weight in response to S217879 treatment (maximum already reached at 3 mg/kg). In a separate experiment, we

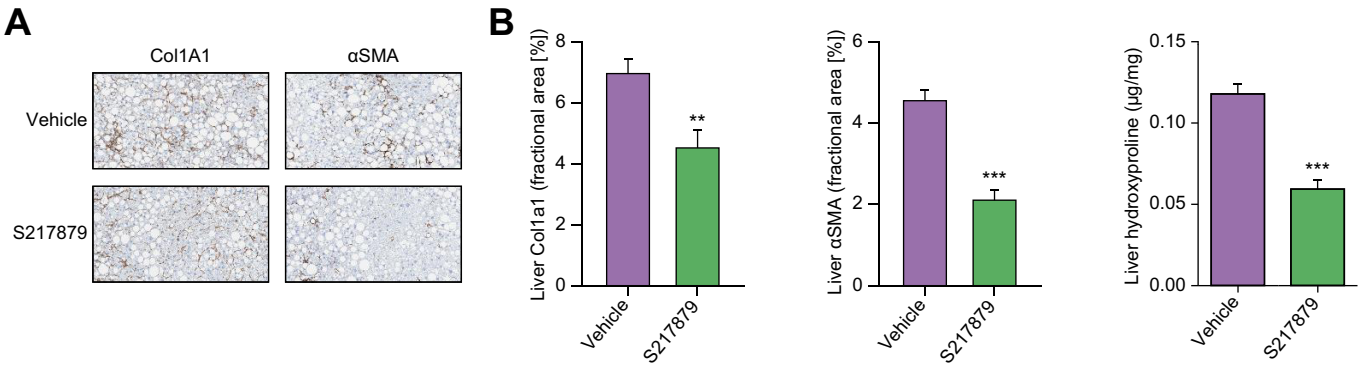

Fig. 6. Markers of liver fibrosis are reduced in response to S217879 treatment in DIO NASH mice. (A) Col1A1- and αSMA-stained liver sections at termination (n = 14 per group). (B) Quantification of Col1A1- and αSMA-positive areas by morphometry. Liver hydroxyproline levels quantified after extraction and centrifugation using a colorimetric assay. Data expressed as mean ± SEM. Significant differences were analyzed using Student's *t* test. ***p <0.001 and **p <0.01: S217879-treated *vs.* vehicle.

performed a full dose response analysis to determine the minimal effective dose in this model (see Fig. S5). Indeed, S217879 treatment prevented disease progression in a dose-dependent manner as shown by reduced NAS and induction of hepatic *Nqo1* expression (Fig. S5AB). The minimal effective dose was set at 1 mg/kg/day in this model. Taken together, these results suggest that S217879-mediated NRF2 activation may provide hepatoprotective properties.

Despite its utility for drug discovery, the MCDD mouse model poorly recapitulates the human NASH etiology with its substantial weight loss and lack of insulin resistance (See[55,58] for review). Nevertheless, results from the basic characterization of S217879 responses in the MCDD model (Fig. 4, Figs. S2–5) prompted us to further document the potential of S217879 for the treatment of NASH in the DIO NASH mouse model in a therapeutic setting. This model has been shown to have a good clinical translatability with respect to the histopathological, transcriptional and metabolic aspects of the human disease.[59] 5–6-week-old C57BL/6JRj mice were fed the DIO NASH diet for 33 weeks prior to initiation of the treatment protocol. Following a liver biopsy for inclusion (see methods), mice were randomized to receive either S217879 (30 mg/kg, PO, QD) or vehicle (HEC 1%) for 8 weeks while being maintained on the DIO NASH diet. S217879 treatment had no impact on food intake (Fig. S6) and body weight (Fig. 5A). It led to a significant reduction of established liver injury as measured by reduced alanine and aspartate aminotransferase (Fig. 5C-D). However, we noticed again a small but significant increase in liver weight in response to treatment (Fig. 5B). Biochemical analyses indicated a reduction in liver triglyceride levels (Fig. 5E). Histological analyses revealed a significant reduction in lobular inflammation resulting in a significant reduction in NAS (Fig. 5G-H, Table S6). These data were confirmed by the decrease of galectin-3 staining (Fig. 5F), a marker of hepatic inflammation.[60,61] Interestingly, S217879 treatment led to a marked reduction in liver fibrosis progression as demonstrated by PSR staining (Fig. 5G-H, Table S6). This reduction in liver fibrosis was independently confirmed by a significant reduction in liver hydroxyproline content (vehicle 0.12 ± 0.017, S217879 0.06 ± 0.014 µg/mg liver, p <0.001) and reduced liver collagen 1A1 and αSMA staining (Fig. 6A-B). Taken together, these results indicate that S217879 treatment led to significant improvements of established NASH and decreased liver fibrosis.

In order to dissect the molecular mechanisms by which S217879-mediated NRF2 activation resulted in reduced NASH and fibrosis progression, RNA-sequencing analysis was performed on liver total RNA at the end of the study. 740 genes were found differentially expressed (361 up and 379 down) between S217879 and vehicle-treated animals (Log_2 fold-change >1, false discovery rate-adjusted p value<0.05, Fig. 7A). These transcriptional changes were further explored by gene set-enrichment analysis (Fig. 7B) which confirmed, as expected, that the NRF2-mediated oxidative stress response was ranked among the most affected pathways in response to treatment ("reactive oxygen species pathway", Fig. 7B) with strong enrichment in NRF2 target genes found upregulated (Fig. 7B–C, Figs. S7–8). The clear and marked upregulation of the overall NRF2 pathway as shown by increased *Nqo1, Gstm1, Gclc* and *Gpx2* expression (Figs. S7–8) demonstrates again that S217879 is a potent NRF2 activator *in vivo*. More interestingly, key pathways involved in NASH pathophysiology related to inflammation ("inflammatory response", "TNFA signaling") and fibrosis ("epithelial mesenchymal transition") were found significantly suppressed in response to treatment (Fig. 7B-E). In line with the reduction of liver inflammation (Fig. 5), we did record the inhibition of several proinflammatory genes such as Mapk4 (Figs. S7–8). Furthermore, a large number of genes associated with fibrosis and stellate cell activation were downregulated, such as *Col1a1, Itgax, Lox* and *Bmp8b* (Figs. S7–8). Again, this is consistent with the significant reduction in liver fibrosis measured in response to treatment. Finally, the expression of several key genes involved in *de novo* lipogenesis was also significantly downregulated (Fig. S8) which is consistent with the anti-steatotic effects of S217879 in this model (Fig. 5E). Taken together, our RNA-sequencing data confirmed that NRF2 activation leads to the upregulation of the antioxidant response and the coordinated regulation of a wide spectrum of genes involved with disease progression, ultimately leading to reduced NASH and liver fibrosis progression.

Discussion

In this manuscript, we reported the identification and detailed characterization of S217879 as a novel, potent and selective compound activating the NRF2 pathway. This compound selectively binds to KEAP1 leading to the disruption of the KEAP1-NRF2 interaction resulting in NRF2 nuclear translocation and

subsequent gene regulation. Moreover, we found that S217879 exhibits an excellent selectivity profile (Table S2) resulting in an excellent safety profile *in vitro* (LD_{50} in HepG2 cells >30 μM) in contrast to potent first-generation compounds such as bardoxolone (LD_{50} in HepG2 cells <1 μM). One key feature of this molecule is its good oral bioavailability which is a major differentiation with respect to first-generation compounds previously identified which displayed good potency and cellular activity but suffered from poor absorption, limited distribution and low metabolic stability (See[30] for review). By contrast, we showed that single oral administration of S217879 resulted in marked target engagement as measured by increased *Nqo1* mRNA levels in the liver (Fig. S1AB) but also in the kidney (data not shown). Furthermore, we found S217879 to be efficacious in the MCDD mouse model at doses as low as 1 mg/kg/day. These data strongly indicate that S217879 is an excellent compound to probe NRF2 biology in preclinical disease models.

In this study, we have shown using two different preclinical models that selective NRF2 activation is beneficial for the treatment of NASH and liver fibrosis. S217879 treatment led to marked reduction in both steatosis and inflammation, resulting in a lower NAS (Figs 4-6). Furthermore, S217879 treatment led to a marked reduction in liver fibrosis in DIO NASH mice, as measured by reduced PSR, Col1A1, and αSMA staining as well reduced hydroxyproline content (Figs 5-6). These data are consistent with histological improvements observed in response to first-generation NRF2 activators, such as TBE-31 and omaveloxolone, in high-fat high-fructose diet-fed mice[37] and STAM mice,[38] respectively. To our knowledge, this is the first report of beneficial properties of a non-covalent NRF2 activator for the treatment NASH and fibrosis. RNA-sequencing analyses indicated that NRF2 activation led to the upregulation of the antioxidant response and the coordinated regulation of a wide spectrum of genes involved with disease progression (Figs. S7–8, Fig. 7). We did observe a pronounced impact on genes belonging to the *de novo* lipogenesis pathway in line with previous observations.[32,62,63] This is in line with the marked reduction in liver triglyceride levels (Fig. 5E). In addition to the expected impact on inflammation (Fig. 5F), one of the most remarkable results obtained in this manuscript is the anti-fibrotic properties of S217879 *in vivo* as measured at the histological, biochemical and gene expression levels (Figs 5-7). This is of major interest since long-term follow-up studies revealed that fibrosis is the main driver of mortality in NASH.[6,7] NRF2 activation may trigger the reduction of liver fibrosis via multiple mechanisms. First, hepatocyte-specific activation of NRF2 has recently been shown to control fibrogenesis during NASH by regulating, at least in part, the antioxidant stress response and thereby reducing DNA damage and apoptosis.[15] Second, NRF2 activation may limit profibrotic macrophage-derived inflammation by negatively interfering with both NF-κB and YAP/NLRP3 pathways.[54,64] Finally, NRF2 has been shown to protect hepatic stellate cells from TGF-β-mediated cell activation[65] suggesting direct anti-fibrotic properties. Our data are consistent with a model in which S217879-induced NRF2 activation reduces NASH progression and slows down the development of liver fibrosis by targeting both parenchymal and non-parenchymal cells (immune cells and stellate cells mainly) as suggested by cell-specific gain (*Keap1* gene deletion) or loss of function (*NRF2* gene deletion) studies,[15,64] respectively. Additional studies using single cell RNA-sequencing analyses or spatial transcriptomics are required to further document the molecular mechanisms at the cellular level and determine the potential contribution of other relevant cell populations, such as liver sinusoidal endothelial cells[66] to S217879-mediated beneficial properties on NASH and fibrosis. Finally, NRF2 activation has been shown to improve gut barrier integrity,[67] which may to some extent contribute to the beneficial impact on NASH progression.[68]

NRF2 activity is reduced during aging[69] and considered as an attractive target for a number of chronic diseases including but not limited to autoimmune, respiratory, neurodegenerative, and cardio-metabolic diseases (See[30] for review). However, it has also been shown to exert both anti-tumorigenic and pro-tumorigenic actions. It is believed that low NRF2 activity may facilitate the initiation of carcinogenesis, whereas constant high activity may drive cancer progression and resistance to chemotherapy.[70] Notably, more than 10% of all hepatocellular carcinomas present a mutation in either *KEAP1* or *NRF2*.[71] Interestingly, we found that treatment with S217879 led to small but significant increase in liver weight in both MCDD and DIO NASH models (Figs 4B-5B). Similar observations were also made in both rats and mice on chow diet exposed to similar drug levels (data not shown). These results are reminiscent of the phenotype of KEAP1-deficient mice suggesting that constitutive NRF2 activation may trigger hepatomegaly.[15,72,73] Notably, constitutive hepatocyte-specific NRF2 activation was shown to significantly reduce NASH-associated hepatocellular carcinoma development in mice with hepatocyte-specific NEMO deficiency.[15] Furthermore, He and colleagues reported that NRF2 forced expression leads to hepatomegaly by, at least in part, increasing the expression of several growth factors such as PDGF and EGF in an AKT-dependent manner.[74] By contrast, we failed to detect any impact on cell proliferation *in vivo* and genes related to cell cycle/proliferation (including the gene signature identified by He and colleagues[74] [*Aurka, Foxm1, Ccnb2, Cdc25b* and *Cdc25c*]) were not significantly modulated upon treatment with S217879 (Fig. 7). Furthermore, *in vitro* studies performed with S217879 tested up to 10 μM (roughly 500-fold higher than NRF2 cell potency) failed to reveal any impact on cell proliferation using HepG2 cells. Finally, we did not detect any AKT phosphorylation in both hepatocytes and HepG2 cells in response to high concentrations of S217879 (data not shown). Obviously, pharmacological activation of NRF2 with a small molecule *in vivo* is not equivalent to NRF2 forced expression[74] or constitutive NRF2 activation by *KEAP1* gene deletion.[15,72,73] As a matter of fact, using a different genetic strategy, Kohler and colleagues created a mouse line with constitutive NRF2 activation in hepatocytes. Surprisingly, these mice did not have any increase in liver weight compared to wild-type mice despite a significant increase in NRF2-regulated gene expression.[75] Taken together, these independent studies suggest that different levels of NRF2 activation due to either constitutive expression or pharmacological activation may result in different phenotypes. Interestingly, Chan *et al.* recently reported that NRF2 pharmacological activation may enhance liver regeneration in mice by supporting hepatocellular hypertrophy.[76] Preliminary evaluation of S217879's safety profile using non-GLP (good laboratory practice) dose-ranging studies in both rats and non-human primates did not reveal any major toxicity. Histological analyses confirmed hepatocellular hypertrophy in rodents as measured by reduced nuclei density (data not shown). Additional studies including GLP-toxicology are required to confirm these preliminary findings and determine the long-term safety of S217879-mediated NRF2 activation.

Abbreviations

ARE, antioxidant response element; DIO, diet-induced obesity; HEC, hydroxyethyl cellulose; hPBMCs, human peripheral blood mononuclear cells; KEAP1, Kelch-like ECH associated protein 1; LPS, lipopolysaccharide; MCDD, methionine- and choline-deficient diet; NAFLD, non-alcoholic fatty liver disease; NAS, NAFLD activity score; NASH, non-alcoholic steatohepatitis; NRF2, nuclear factor erythroid 2–related factor 2; PSR, Picrosirius red; ROS, reactive oxygen species; GSEA, Gene Set Enrichment Analysis; HSCs, Hepatic Stellate Cells; PPI, Protein-protein interaction; 4-HNE, 4-hydroxynonenal.

Financial support

This work was funded by Institut de Recherches Servier.

Conflicts of interest

All the authors are/were employees of Servier.

Please refer to the accompanying ICMJE disclosure forms for further details.

Authors' contributions

KS and PD coordinated the work. SC, OB, AG, CI, AH, JR and KL performed the *in vitro* and *in vivo* studies. VD, NP, KS, PD, CV, SB, VP and LMV contributed to experimental design and data interpretation. CW supervised the medicinal chemistry program (design and synthesis) with the help of AK and DD. VM was responsible for molecular modelling, NM for scale-up syntheses. FM performed bioinformatic analyses. CW and PD drafted the manuscript.

Data availability statement

The data that support the findings of this study are available from the corresponding author upon reasonable request.

Acknowledgments

We would like to thank Michael Feigh and the team at GUBRA (Hørsholm, Denmark) for their excellent support regarding the DIO NASH study.

Supplementary data

Supplementary data to this article can be found online at https://doi.org/10.1016/j.jhepr.2022.100651.

References

Author names in bold designate shared co-first authorship

[1] Brunt EM, Wong VWS, Nobili V, Day CP, Sookoian S, Maher JJ, et al. Nonalcoholic fatty liver disease. Nat Rev Dis Prim 2015:1; https://doi.org/10.1038/nrdp.2015.80.

[2] Diehl AM, Day C. Cause, pathogenesis, and treatment of nonalcoholic steatohepatitis. N Engl J Med 2017;377:2063–2072; https://doi.org/10.1056/nejmra1503519.

[3] Younossi ZM, Golabi P, de Avila L, Paik JM, Srishord M, Fukui N, et al. The global epidemiology of NAFLD and NASH in patients with type 2 diabetes: a systematic review and meta-analysis. J Hepatol 2019;71:793–801; https://doi.org/10.1016/j.jhep.2019.06.021.

[4] Younossi ZM, Koenig AB, Abdelatif D, Fazel Y, Henry L, Wymer M. Global epidemiology of nonalcoholic fatty liver disease—meta-analytic assessment of prevalence, incidence, and outcomes. Hepatology 2016;64:73–84; https://doi.org/10.1002/hep.28431.

[5] **Loomba R**, **Friedman SL**, **Shulman GI**. Mechanisms and disease consequences of nonalcoholic fatty liver disease. Cell 2021;184:2537–2564; https://doi.org/10.1016/j.cell.2021.04.015.

[6] Angulo P, Kleiner DE, Dam-Larsen S, Adams LA, Bjornsson ES, Charatcharoenwitthaya P, et al. Liver fibrosis, but no other histologic features, is associated with long-term outcomes of patients with nonalcoholic fatty liver disease. Gastroenterology 2015;149:389–397.e10; https://doi.org/10.1053/j.gastro.2015.04.043.

[7] Hagström H, Nasr P, Ekstedt M, Hammar U, Stål P, Hultcrantz R, et al. Risk for development of severe liver disease in lean patients with nonalcoholic fatty liver disease: a long-term follow-up study. Hepatol Commun 2018;2:48–57; https://doi.org/10.1002/hep4.1124.

[8] Romero FA, Jones CT, Xu Y, Fenaux M, Halcomb RL. The race to bash NASH: emerging targets and drug development in a complex liver disease. J Med Chem 2020; https://doi.org/10.1021/acs.jmedchem.9b01701.

[9] Anstee QM, Day CP. The genetics of NAFLD. Nat Rev Gastroenterol Hepatol 2013;10:645–655; https://doi.org/10.1038/nrgastro.2013.182.

[10] Trépo E, Valenti L. Update on NAFLD genetics: from new variants to the clinic. J Hepatol 2020;72:1196–1209; https://doi.org/10.1016/j.jhep.2020.02.020.

[11] Arroyave-Ospina JC, Wu Z, Geng Y, Moshage H. Role of oxidative stress in the pathogenesis of non-alcoholic fatty liver disease: implications for prevention and therapy. Antioxidants (Basel, Switzerland) 2021;10:1–25; https://doi.org/10.3390/ANTIOX10020174.

[12] Madan K, Bhardwaj P, Thareja S, Gupta SD, Saraya A. Oxidant stress and antioxidant status among patients with nonalcoholic fatty liver disease (NAFLD). J Clin Gastroenterol 2006;40:930–935; https://doi.org/10.1097/01.MCG.0000212608.59090.08.

[13] Palmieri VO, Grattagliano I, Portincasa P, Palasciano G. Systemic oxidative alterations are associated with visceral adiposity and liver steatosis in patients with metabolic syndrome. J Nutr 2006;136:3022–3026; https://doi.org/10.1093/JN/136.12.3022.

[14] Podszun MC, Chung JY, Ylaya K, Kleiner DE, Hewitt SM, Rotman Y. 4-HNE immunohistochemistry and image analysis for detection of lipid peroxidation in human liver samples using vitamin E treatment in NAFLD as a proof of concept. J Histochem Cytochem 2020;68:635–643; https://doi.org/10.1369/0022155420946402.

[15] Mohs A, Otto T, Schneider KM, Peltzer M, Boekschoten M, Holland CH, et al. Hepatocyte-specific NRF2 activation controls fibrogenesis and carcinogenesis in steatohepatitis. J Hepatol 2021;74:638–648; https://doi.org/10.1016/J.JHEP.2020.09.037.

[16] Masarone M, Rosato V, Dallio M, Gravina AG, Aglitti A, Loguercio C, et al. Role of oxidative stress in pathophysiology of nonalcoholic fatty liver disease. Oxid Med Cell Longev 2018;2018. https://doi.org/10.1155/2018/9547613.

[17] Satapati S, Kucejova B, Duarte JAG, Fletcher JA, Reynolds L, Sunny NE, et al. Mitochondrial metabolism mediates oxidative stress and inflammation in fatty liver. J Clin Invest 2015;125:4447–4462; https://doi.org/10.1172/JCI82204.

[18] Koliaki C, Szendroedi J, Kaul K, Jelenik T, Nowotny P, Jankowiak F, et al. Adaptation of hepatic mitochondrial function in humans with non-alcoholic fatty liver is lost in steatohepatitis. Cell Metab 2015;21:739–746; https://doi.org/10.1016/J.CMET.2015.04.004.

[19] Karkucinska-Wieckowska A, Simoes ICM, Kalinowski P, Lebiedzinska-Arciszewska M, Zieniewicz K, Milkiewicz P, et al. Mitochondria, oxidative stress and nonalcoholic fatty liver disease: a complex relationship. Eur J Clin Invest 2022:52; https://doi.org/10.1111/ECI.13622.

[20] Dodson M, De La Vega MR, Cholanians AB, Schmidlin CJ, Chapman E, Zhang DD. Modulating NRF2 in disease: timing is everything. Annu Rev Pharmacol Toxicol 2019;59:555–575; https://doi.org/10.1146/ANNUREV-PHARMTOX-010818-021856.

[21] Tong KI, Katoh Y, Kusunoki H, Itoh K, Tanaka T, Yamamoto M. Keap1 recruits Neh2 through binding to ETGE and DLG motifs: characterization of the two-site molecular recognition model. Mol Cell Biol 2006;26:2887–2900; https://doi.org/10.1128/mcb.26.8.2887-2900.2006.

[22] Tong KI, Padmanabhan B, Kobayashi A, Shang C, Hirotsu Y, Yokoyama S, et al. Different electrostatic potentials define ETGE and DLG motifs as hinge and latch in oxidative stress response. Mol Cell Biol 2007;27:7511–7521; https://doi.org/10.1128/MCB.00753-07.

[23] Zhang DD, Hannink M. Distinct cysteine residues in Keap1 are required for Keap1-dependent ubiquitination of Nrf2 and for stabilization of Nrf2 by chemopreventive agents and oxidative stress. Mol Cell Biol 2003;23:8137–8151; https://doi.org/10.1128/MCB.23.22.8137-8151.2003.

[24] Zhang DD, Lo S-C, Cross JV, Templeton DJ, Hannink M. Keap1 is a redox-regulated substrate adaptor protein for a Cul3-dependent ubiquitin ligase complex. Mol Cell Biol 2004;24:10941–10953; https://doi.org/10.1128/MCB.24.24.10941-10953.2004.

[25] Eggler AL, Small E, Hannink M, Mesecar AD. Cul3-mediated Nrf2 ubiquitination and antioxidant response element (ARE) activation are dependent on the partial molar volume at position 151 of Keap1. Biochem J 2009;422:171–180; https://doi.org/10.1042/BJ20090471.

[26] Wakabayashi N, Dinkova-Kostova AT, Holtzclaw WD, Kang-Il M, Kobayashi A, Yamamoto M, et al. Protection against electrophile and oxidant stress by induction of the phase 2 response: fate of cysteines of the Keap1 sensor modified by inducers. Proc Natl Acad Sci U S A 2004;101:2040–2045; https://doi.org/10.1073/PNAS.0307301101.

[27] Itoh K, Chiba T, Takahashi S, Ishii T, Igarashi K, Katoh Y, et al. An Nrf2/small Maf heterodimer mediates the induction of phase II detoxifying enzyme genes through antioxidant response elements. Biochem Biophys Res Commun 1997;236:313–322; https://doi.org/10.1006/BBRC.1997.6943.

[28] Marini MG, Chan K, Casula L, Kan YW, Cao A, Moi P. hMAF, a small human transcription factor that heterodimerizes specifically with Nrf1 and Nrf2. J Biol Chem 1997;272:16490–16497; https://doi.org/10.1074/JBC.272.26.16490.

[29] Hayes JD, Dinkova-Kostova AT. The Nrf2 regulatory network provides an interface between redox and intermediary metabolism. Trends Biochem Sci 2014;39:199–218; https://doi.org/10.1016/J.TIBS.2014.02.002.

[30] Cuadrado A, Rojo AI, Wells G, Hayes JD, Cousin SP, Rumsey WL, et al. Therapeutic targeting of the NRF2 and KEAP1 partnership in chronic diseases. Nat Rev Drug Discov 2019;18:295–317; https://doi.org/10.1038/S41573-018-0008-X.

[31] Tang W, Jiang YF, Ponnusamy M, Diallo M. Role of Nrf2 in chronic liver disease. World J Gastroenterol 2014;20:13079–13087; https://doi.org/10.3748/WJG.V20.I36.13079.

[32] Meakin PJ, Chowdhry S, Sharma RS, Ashford FB, Walsh SV, McCrimmon RJ, et al. Susceptibility of Nrf2-null mice to steatohepatitis and cirrhosis upon consumption of a high-fat diet is associated with oxidative stress, perturbation of the unfolded protein response, and disturbance in the expression of metabolic enzymes but not with insulin resistance. Mol Cell Biol 2014;34:3305–3320; https://doi.org/10.1128/MCB.00677-14.

[33] Chowdhry S, Nazmy MH, Meakin PJ, Dinkova-Kostova AT, Walsh SV, Tsujita T, et al. Loss of Nrf2 markedly exacerbates nonalcoholic steatohepatitis. Free Radic Biol Med 2010;48:357–371; https://doi.org/10.1016/J.FREERADBIOMED.2009.11.007.

[34] **Sugimoto H**, **Okada K**, Shoda J, Warabi E, Ishige K, Ueda T, et al. Deletion of nuclear factor-E2-related factor-2 leads to rapid onset and progression of nutritional steatohepatitis in mice. Am J Physiol - Gastrointest Liver Physiol 2010:298; https://doi.org/10.1152/ajpgi.00296.2009.

[35] Okada K, Warabi E, Sugimoto H, Horie M, Tokushige K, Ueda T, et al. Nrf2 inhibits hepatic iron accumulation and counteracts oxidative stress-induced liver injury in nutritional steatohepatitis. J Gastroenterol 2012;47:924–935; https://doi.org/10.1007/S00535-012-0552-9.

[36] Tanaka Y, Aleksunes LM, Yeager RL, Gyamfi MA, Esterly N, Guo GL, et al. NF-E2-related factor 2 inhibits lipid accumulation and oxidative stress in mice fed a high-fat diet. J Pharmacol Exp Ther 2008;325:655–664; https://doi.org/10.1124/jpet.107.135822.

[37] Sharma RS, Harrison DJ, Kisielewski D, Cassidy DM, McNeilly AD, Gallagher JR, et al. Experimental nonalcoholic steatohepatitis and liver fibrosis are ameliorated by pharmacologic activation of Nrf2 (NF-E2 p45-related factor 2). Cell Mol Gastroenterol Hepatol 2018;5:367–398. https://doi.org/10.1016/j.jcmgh.2017.11.016.

[38] Reisman SA, Ferguson DA, Lee CYI, Proksch JW. Omaveloxolone and TX63682 are hepatoprotective in the STAM mouse model of nonalcoholic steatohepatitis. J Biochem Mol Toxicol 2020;2020:34; https://doi.org/10.1002/JBT.22526.

[39] Azzimato V, Jager J, Chen P, Morgantini C, Levi L, Barreby E, et al. Liver macrophages inhibit the endogenous antioxidant response in obesity-associated insulin resistance. Sci Transl Med 2020;12; https://doi.org/10.1126/SCITRANSLMED.AAW9709.

[40] Bricambert J, Alves-Guerra MC, Esteves P, Prip-Buus C, Bertrand-Michel J, Guillou H, et al. The histone demethylase Phf2 acts as a molecular checkpoint to prevent NAFLD progression during obesity. Nat Commun 2018:9; https://doi.org/10.1038/S41467-018-04361-Y.

[41] Yore MM, Kettenbach AN, Sporn MB, Gerber SA, Liby KT. Proteomic analysis shows synthetic oleanane triterpenoid binds to mTOR. PLoS One 2011;6; https://doi.org/10.1371/JOURNAL.PONE.0022862.

[42] de Zeeuw D, Akizawa T, Audhya P, Bakris GL, Chin M, Christ-Schmidt H, et al. Bardoxolone methyl in type 2 diabetes and stage 4 chronic kidney disease. N Engl J Med 2013;369:2492–2503; https://doi.org/10.1056/NEJMOA1306033.

[43] Chin MP, Wrolstad D, Bakris GL, Chertow GM, De Zeeuw D, Goldsberry A, et al. Risk factors for heart failure in patients with type 2 diabetes mellitus and stage 4 chronic kidney disease treated with bardoxolone methyl. J Card Fail 2014;20:953–958; https://doi.org/10.1016/J.CARDFAIL.2014.10.001.

[44] Li X, Zhang D, Hannink M, Beamer LJ. Crystal structure of the Kelch domain of human Keap1. J Biol Chem 2004;279:54750–54758; https://doi.org/10.1074/JBC.M410073200.

[45] Schmoll D, Engel CK, Glombik H. The Keap1–Nrf2 protein–protein interaction: a suitable target for small molecules. Drug Discov Today Tech 2017;24:11–17. https://doi.org/10.1016/j.ddtec.2017.10.001.

[46] Davies TG, Wixted WE, Coyle JE, Griffiths-Jones C, Hearn K, McMenamin R, et al. Monoacidic inhibitors of the Kelch-like ECH-associated protein 1: nuclear factor erythroid 2-related factor 2 (KEAP1:NRF2) protein-protein interaction with high cell potency identified by fragment-based discovery. J Med Chem 2016;59:3991–4006; https://doi.org/10.1021/ACS.JMEDCHEM.6B00228.

[47] Kristiansen MNB, Veidal SS, Rigbolt KTG, Tølbøl KS, Roth JD, Jelsing J, et al. Obese diet-induced mouse models of nonalcoholic steatohepatitis-tracking disease by liver biopsy. World J Hepatol 2016;8:673; https://doi.org/10.4254/WJH.V8.I16.673.

[48] Kleiner DE, Brunt EM, Van Natta M, Behling C, Contos MJ, Cummings OW, et al. Design and validation of a histological scoring system for nonalcoholic fatty liver disease. Hepatology 2005;41:1313–1321; https://doi.org/10.1002/hep.20701.

[49] Morel PS, Duvivier V, Bertin F, Provost N, Hammoutene A, Hubert EL, et al. Procollagen C-Proteinase Enhancer-1 (PCPE-1) deficiency in mice reduces liver fibrosis but not NASH progression. PLoS One 2022;17:e0263828; https://doi.org/10.1371/JOURNAL.PONE.0263828.

[50] Tran KT, Pallesen JS, Solbak SM, Narayanan D, Baig A, Zang J, et al. A comparative assessment study of known small-molecule Keap1-Nrf2 protein-protein interaction inhibitors: chemical synthesis, binding properties, and cellular activity. J Med Chem 2019;62:8028–8052; https://doi.org/10.1021/ACS.JMEDCHEM.9B00723/SUPPL_FILE/JM9B00723_SI_002.CSV.

[51] Ma B, Lucas B, Capacci A, Lin EYS, Jones JH, Dechantsreiter M, et al. Design, synthesis and identification of novel, orally bioavailable non-covalent Nrf2 activators. Bioorg Med Chem Lett 2020;30:126852; https://doi.org/10.1016/J.BMCL.2019.126852.

[52] Mallinson J, Collins I. Macrocycles in new drug discovery. Future Med Chem 2012;4:1409–1438; https://doi.org/10.4155/FMC.12.93/ASSET/IMAGES/LARGE/FIGURE49.JPEG.

[53] **Wen Wong DP**, **Ng MY**, Leung JY, Boh BK, Lim EC, Tan SH, et al. Regulation of the NRF2 transcription factor by andrographolide and organic extracts from plant endophytes. PLoS One 2018;13:e0204853; https://doi.org/10.1371/JOURNAL.PONE.0204853.

[54] Kobayashi EH, Suzuki T, Funayama R, Nagashima T, Hayashi M, Sekine H, et al. Nrf2 suppresses macrophage inflammatory response by blocking proinflammatory cytokine transcription. Nat Commun 2016;7; https://doi.org/10.1038/NCOMMS11624.

[55] Santhekadur PK, Kumar DP, Sanyal AJ. Preclinical models of non-alcoholic fatty liver disease. J Hepatol 2018;68:230–237; https://doi.org/10.1016/j.jhep.2017.10.031.

[56] Machado MV, Michelotti GA, Xie G, De Almeida TP, Boursier J, Bohnic B, et al. Mouse models of diet-induced nonalcoholic steatohepatitis reproduce the heterogeneity of the human disease. PLoS One 2015;10:e0127991; https://doi.org/10.1371/JOURNAL.PONE.0127991.

[57] Lickteig AJ, Fisher CD, Augustine LM, Cherrington NJ. Genes of the antioxidant response undergo upregulation in a rodent model of nonalcoholic steatohepatitis. J Biochem Mol Toxicol 2007;21:216–220; https://doi.org/10.1002/JBT.20177.

[58] Rinella ME, Green RM. The methionine-choline deficient dietary model of steatohepatitis does not exhibit insulin resistance. J Hepatol 2004;40:47–51; https://doi.org/10.1016/J.JHEP.2003.09.020.

[59] Hansen HH, Ægidius HM, Oró D, Evers SS, Heebøll S, Eriksen PL, et al. Human translatability of the GAN diet-induced obese mouse model of non-alcoholic steatohepatitis. BMC Gastroenterol 2020;20; https://doi.org/10.1186/s12876-020-01356-2.

[60] Henderson NC, Mackinnon AC, Farnworth SL, Poirier F, Russo FP, Iredale JP, et al. Galectin-3 regulates myofibroblast activation and hepatic fibrosis. Proc Natl Acad Sci U S A 2006;103:5060–5065; https://doi.org/10.1073/PNAS.0511167103.

[61] **Iacobini C**, **Menini S**, **Ricci C**, Fantauzzi CB, Scipioni A, Salvi L, et al. Galectin-3 ablation protects mice from diet-induced NASH: a major scavenging role for galectin-3 in liver. J Hepatol 2011;54:975–983; https://doi.org/10.1016/J.JHEP.2010.09.020.

[62] Slocum SL, Skoko JJ, Wakabayashi N, Aja S, Yamamoto M, Kensler TW, et al. Keap1/Nrf2 pathway activation leads to a repressed hepatic gluconeogenic and lipogenic program in mice on a high-fat diet. Arch Biochem Biophys 2016;591:57–65; https://doi.org/10.1016/J.ABB.2015.11.040.

[63] **Knatko EV**, **Tatham MH**, Zhang Y, Castro C, Higgins M, Dayalan Naidu S, et al. Downregulation of Keap1 confers features of a fasted metabolic state. IScience 2020;2020:23; https://doi.org/10.1016/J.ISCI.2020.101638.

[64] **Wang P**, **Ni M**, **Tian Y**, Wang H, Qiu J, You W, et al. Myeloid Nrf2 deficiency aggravates non-alcoholic steatohepatitis progression by regulating YAP-

mediated NLRP3 inflammasome signaling. IScience 2021;24; https://doi.org/10.1016/J.ISCI.2021.102427.
[65] Prestigiacomo V, Suter-Dick L. Nrf2 protects stellate cells from Smad-dependent cell activation. PLoS One 2018;13; https://doi.org/10.1371/JOURNAL.PONE.0201044.
[66] Furuta K, Guo Q, Hirsova P, Ibrahim SH. Emerging roles of liver sinusoidal endothelial cells in nonalcoholic steatohepatitis. Biol 2020;9:395; https://doi.org/10.3390/BIOLOGY9110395.
[67] Singh R, Chandrashekharappa S, Bodduluri SR, Baby BV, Hegde B, Kotla NG, et al. Enhancement of the gut barrier integrity by a microbial metabolite through the Nrf2 pathway. Nat Commun 2019;10; https://doi.org/10.1038/S41467-018-07859-7.
[68] Mouries J, Brescia P, Silvestri A, Spadoni I, Sorribas M, Wiest R, et al. Microbiota-driven gut vascular barrier disruption is a prerequisite for non-alcoholic steatohepatitis development. J Hepatol 2019;71:1216–1228; https://doi.org/10.1016/J.JHEP.2019.08.005.
[69] Schmidlin CJ, Dodson MB, Madhavan L, Zhang DD. Redox regulation by NRF2 in aging and disease. Free Radic Biol Med 2019;134:702–707; https://doi.org/10.1016/J.FREERADBIOMED.2019.01.016.
[70] Kensler TW, Wakabayashi N. Nrf2: friend or foe for chemoprevention? Carcinogenesis 2010;31:90–99; https://doi.org/10.1093/CARCIN/BGP231.
[71] **Schulze K**, **Imbeaud S**, **Letouzé E**, Alexandrov LB, Calderaro J, Rebouissou S, et al. Exome sequencing of hepatocellular carcinomas identifies new mutational signatures and potential therapeutic targets. Nat Genet 2015;47:505–511; https://doi.org/10.1038/ng.3252.
[72] Okawa H, Motohashi H, Kobayashi A, Aburatani H, Kensler TW, Yamamoto M. Hepatocyte-specific deletion of the keap1 gene activates Nrf2 and confers potent resistance against acute drug toxicity. Biochem Biophys Res Commun 2006;339:79–88; https://doi.org/10.1016/J.BBRC.2005.10.185.
[73] Komatsu M, Kurokawa H, Waguri S, Taguchi K, Kobayashi A, Ichimura Y, et al. The selective autophagy substrate p62 activates the stress responsive transcription factor Nrf2 through inactivation of Keap1. Nat Cell Biol 2010;12:213–223; https://doi.org/10.1038/ncb2021.
[74] **He F**, **Antonucci L**, **Yamachika S**, Zhang Z, Taniguchi K, Umemura A, et al. NRF2 activates growth factor genes and downstream AKT signaling to induce mouse and human hepatomegaly. J Hepatol 2020;72:1182–1195; https://doi.org/10.1016/J.JHEP.2020.01.023.
[75] Köhler UA, Kurinna S, Schwitter D, Marti A, Schäfer M, Hellerbrand C, et al. Activated Nrf2 impairs liver regeneration in mice by activation of genes involved in cell-cycle control and apoptosis. Hepatology 2014;60:670–678; https://doi.org/10.1002/HEP.26964.
[76] **Chan BKY**, **Elmasry M**, **Forootan SS**, Russomanno G, Bunday TM, Zhang F, et al. Pharmacological activation of Nrf2 enhances functional liver regeneration. Hepatology 2021;74:973–986; https://doi.org/10.1002/HEP.31859.

Journal of Hepatology, Volume *5*

Supplemental information

Selective disruption of NRF2-KEAP1 interaction leads to NASH resolution and reduction of liver fibrosis in mice

Klaus Seedorf, Csaba Weber, Cedric Vinson, Sylvie Berger, Laurent-Michel Vuillard, Arpad Kiss, Stephanie Creusot, Olivier Broux, Anne Geant, Catherine Ilic, Karine Lemaitre, Johann Richard, Adel Hammoutene, Julien Mahieux, Virginie Martiny, Didier Durand, Fabien Melchiore, Miklos Nyerges, Valerie Paradis, Nicolas Provost, Valérie Duvivier, and Philippe Delerive

Selective disruption of NRF2-KEAP1 interaction leads to NASH resolution and reduction of liver fibrosis in mice

Klaus Seedorf, Csaba Weber, Cedric Vinson, Sylvie Berger, Laurent-Michel Vuillard, Arpad Kiss, Stephanie Creusot, Olivier Broux, Anne Geant, Catherine Ilic, Karine Lemaitre, Johann Richard, Adel Hammoutene, Julien Mahieux, Virginie Martigny, Didier Durand, Fabien Melchiore, Miklos Nyerges, Valerie Paradis, Nicolas Provost, Valérie Duvivier, Philippe Delerive

Table of contents

Supplementary methods

Surface Plasmon Resonance assay

Binding assay to Kelch domain of KEAP1 was performed by Surface Plasmon resonance (SPR) on a Biacore T200 (GE Healthcare) at 25°C.

Immobilization: HIS-Thromb-KEAP1 (A321-C624) (Novalix, Batch PU-P01; MW:33812.9 Da) is immobilized on the active flow cell of a CM5 chip at a concentration of 40 µg/mL (coupling buffer : 10 mM Na acetate pH 5.5) using the standard wizard method (amine coupling). Amine blank is used as the reference flow cell.

The immobilization buffer is 10 mM Hepes, 150 mM NaCl, 3 mM EDTA pH 7.4, 0.05% P20 (HBS-EP+), 1mM TCEP pH 7.4. Immobilization target is reached at 2500 RU, with a 10 µL/min flowrate and at 25°C.

Response bound (RU) :	FcAct
20170913 N=1	2510 RU
20170913 N=2	2627 RU

Assay: The running buffer is 10 mM Hepes, 150 mM NaCl, 3 mM EDTA pH 7.4, 0.05% P20 (HBSEP) pH 7.4, 1 mM TCEP + 5% DMSO.

Compounds bindings are monitored by Single-Cycle Kinetics (High Performance), with 5 increasing concentrations per cycle. Injection runs for 180 seconds at a 50 µL/min flowrate, dissociation runs for 360 seconds at a 50 µL/min flowrate, both at 25°C. For very slow

dissociation rate, dissociation time was extended to 1h30 to get reliable data. Extra wash after the 5 cycles is a solution of 50% DMSO. Carry-over and solvent correction are applied.

Step	**Solution**	**Time (s)**	**Flowrate (µL/min)**	**Running Buffer**	**# of iteration**
Association Dissociation	S compound Running Buffer	180 360 / 5400	50 50	HBSEP, 1 mM TCEP, 5% DMSO	x5
Extra wash	50% DMSO				

NRF2 translocation assay

PathHunter® U2OS Keap1-NRF2 Nuclear Translocation Cell Line was provided by Eurofins (DiscoverX). PathHunter U2OS cells were grown in Minimum Essential Medium (MEM) (#30-2003, ATCC), 10% FBS (#P30-193306), PanBiotech), 500 µg/ml Geneticine, 250 µg/ml Hygromycine, 0.25 µg/ml Puromycine (10131-027, 10687-010 and A1113802 respectively, Life Technologies). The night before experiment, cells were harvested using Tryple Xpress (Ref.126905, Bibco) for 5min at 37°C, resuspended in Opti-MEM (Ref.31985-047, Gibco), 1% FBS (#P30-193306, Panbiotech) and then plated into 384 well plates (Ref.6007680, Perkin Elmer) at the density of 7,500 cells/well in 20 µl. Cells are stored overnight at 37°C (5% CO2) until used. Compounds in 100% DMSO (0.315 µl/well) were resuspended in 20 µl MEM, 1% FBS, 3.4% DMSO. Compounds and Andrographolide (10 µM final concentration; Ref.365645-500MG, Aldrich) as positive control, were dispensed on cell, 5 µl/well, and then incubated for 3h at 37°C and 5% CO2. After incubation, PathHunter reagents were dispensed on cells (12 µl/well, Ref.93-0001, DiscoverX) and incubated for 60 min at room temperature in the dark.

Then luminescence signal was measured using multimodal reader (Pherastar, BMG Labtech). Data were normalized between 1% DMSO (basal signal) and 10 µM Andrographolide (positive signal) and analyzed using Activity Base software.

HepG2 NRF2 transactivation assay

CellSensor™ ARE-bla Hep G2 Cell Line (#K133) containing a betalactamase reporter gene under control of an ARE was provided by Thermofisher. CellSensor® ARE-bla HepG2 cells were grown to confluence in DMEM GlutaMAXTM (#61965-026, Thermo Fisher), 10% dialyzed FBS (#P30-193306, PanBiotech), 12mM Hepes (#15630-056, Gibco), 0.1mM Non-Essential Amino Acid (NEAA) Cell Culture Supplement (#11140-35, Gibco), 1% Na-pyruvate (#S8636, Sigma), 2.5 µg/ml Blasticidine (#210-01, Invitrogene), 1% Penicilline/streptomycine (15070-063, Gibco) in collagen I (50 µg/ml, #A10483-1, Life technologies) coated flasks, 37°C, 5% CO2. Eighteen hours before the experiment, cells were harvested using TrypleXpress (Ref126905, Bibco) for 10 min at 37°C, resuspended in DMEM GlutaMAXTM (#61965-026, Thermo Fisher), 1% dialyzed FBS (#P30-193306, PanBiotech), 25 mM Hepes (#15630-056, Gibco) 0.1mM NEAA (#11140-35, Gibco), 1% Na-pyruvate (#S8636, Sigma), 2.5 µg/ml Blasticidine (#210-01, Invitrogen), 1% Penicilline/streptomycine (15070-063, Gibco) then plated into 384 wells Cell culture microclear plates (#781091, Greiner) at the density of 30 000 cells/well in 32 µl. Cells are stored at 37°C, 5% CO2 until used. Compounds in 100% DMSO (0.315 µl/well) were resuspended in 20 µl DMEM GlutaMAXTM, 1% dialyzed FBS, 25mM hepes, 0.1mM NEAA, 1% Na-pyruvate (#S8636, Sigma), 2.5 µg/ml Blasticidine, 3.4 % DMSO, 1% Penicilline/streptomycine (15070-063, Gibco). Compounds and Andrographolide (10 µM final concentration, #365645-500MG, Aldrich) as positive control, were dispensed on cell, 8 µl/well, and then incubated for 16h at 37°C and 5% CO2. The day after Live Blazer reagent (Live Blazer FRET B/G (CCF4-M), #K1089, Invitrogen), was dispensed on cells (8 µl/well) and incubated for 2h at room temperature in the dark. Then, Fluorescence Resonance Energy Transfer (FRET)

signal was measured using multimodal reader (Ex 409nM/Em and 530 nM; Envision, Perkin Elmer). Data were normalized between 1% DMSO (basal signal) and 10 µM Andrographolide (positive signal) and analyzed using Activity Base software.

ROS quantification in HepG2 cells

HepG2 cells (ATCC, were seeded at 20,000 cells/well in a 96 well-plate (Dutcher #655090) and cultured in complete medium for 24h. Cells were pre incubated with compounds of interest or vehicle (DMSO 0.1%) for 24h. In order to measure ROS generation, cell culture medium is harvested and replaced by Live-cell imaging medium (Invitrogen #A14291DJ). ROS are then triggered with H2O2 (200µM) for 90min in total. The CM-H2DCFDA probe (Invitrogen #C6827) is added 45 min after H2O2 (Sigma H1009) treatment to the wells for an additional 45 min. Cells are then washed with PBS and Live-cell imaging culture medium is added into the wells. Probe's fluorescence is then read on a Biotek Synergy 2 fluorometer (Ex/Em 492-495/517-527 nm) and results were analyzed using Prism (Graphpad).

Chemical synthesis of compound 3.

Synthesis overview:

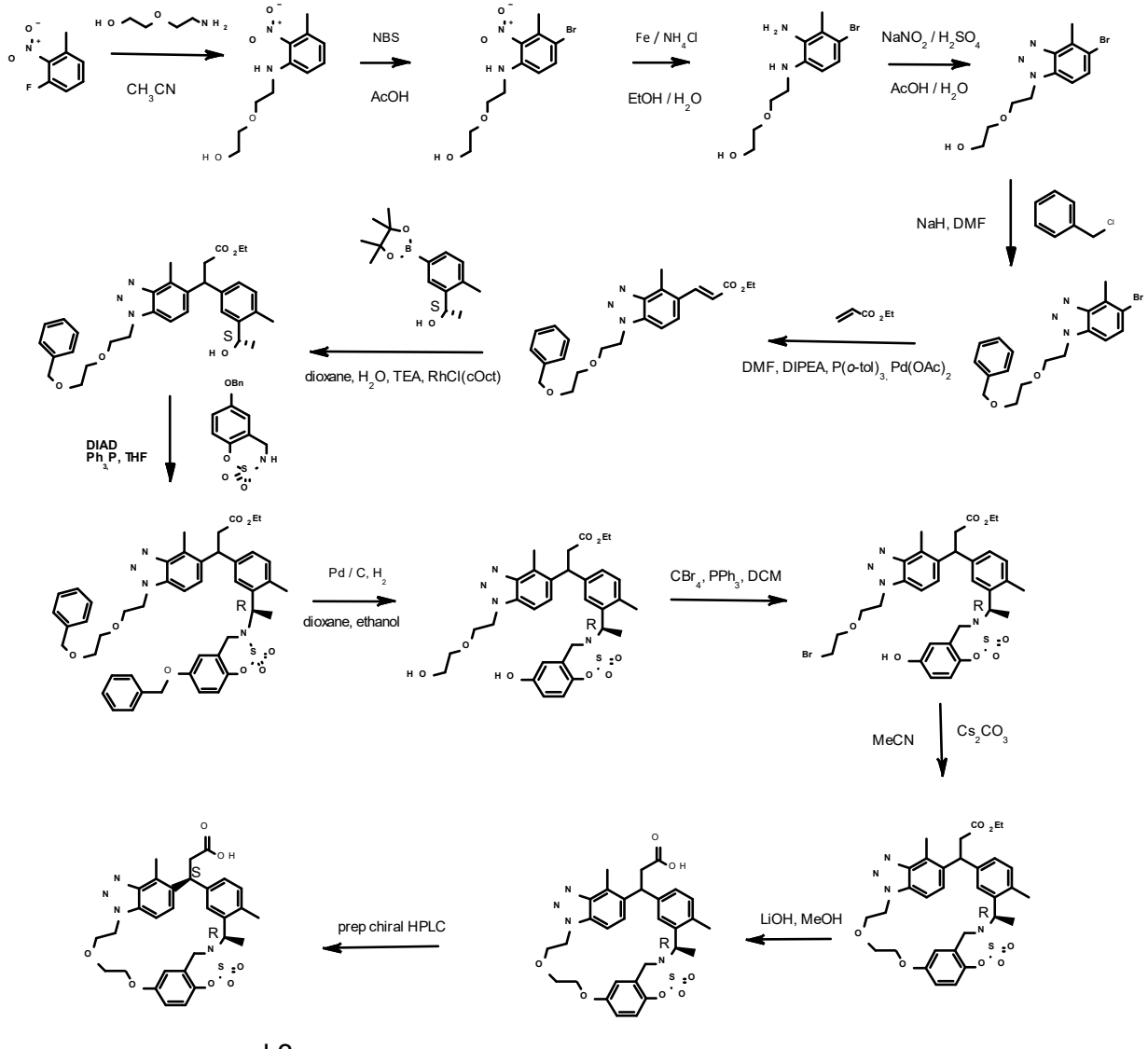

compound 3

Preparation of crystalline form for Xray crystallography: Compound 3 was added at room temperature portion-wise to THF under stirring until suspension was formed. Solid was filtered off, THF was slowly concentrated under decreased pressure. Crystals were filtered off. Absolute configuration of compound 3 was proved with Xray crystallography. Xray crystallography data are uploaded to Cambridge Structural database.

Supplementary figures

Fig. S1: single administration of S217879 (30mg/kg) leads to NRF2 activation *in vivo*. A: Male C57BL/6J mice received a single administration of S217879 (30mg/kg) by gavage in HEC 1% as vehicle. S217879 plasma levels were analyzed by LC-MS/MS. Liver Nqo1 mRNA levels were quantified by RT-qPCR (n=3 per time point). **B**: Male C57BL/6J mice on MCD diet received a single administration of S217879 (30mg/kg) by gavage or vehicle (HEC 1%). 24h post administration, animals were sacrificed by cardiac puncture under isoflurane anesthesia. Liver samples were collected for gene expression studies by RT-qPCR. (*: p<0.05 treated vs. vehicle; n=3 per group).

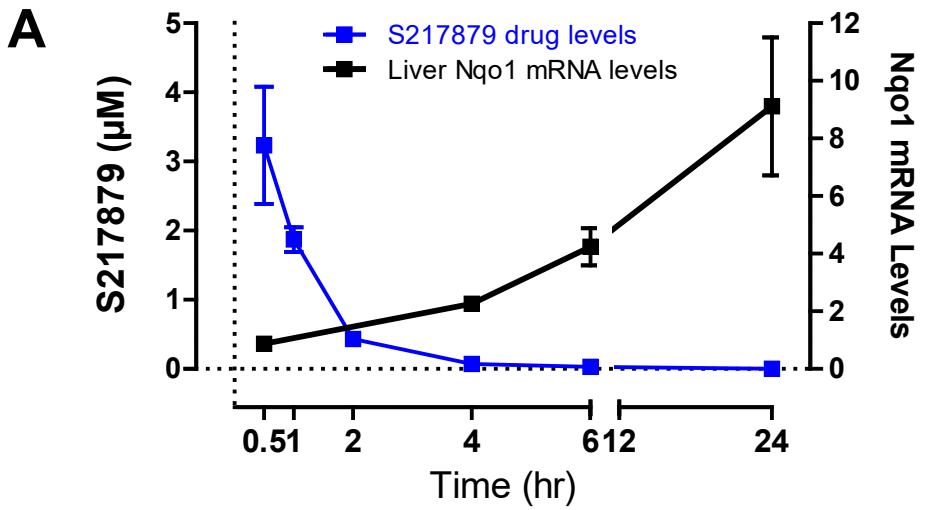

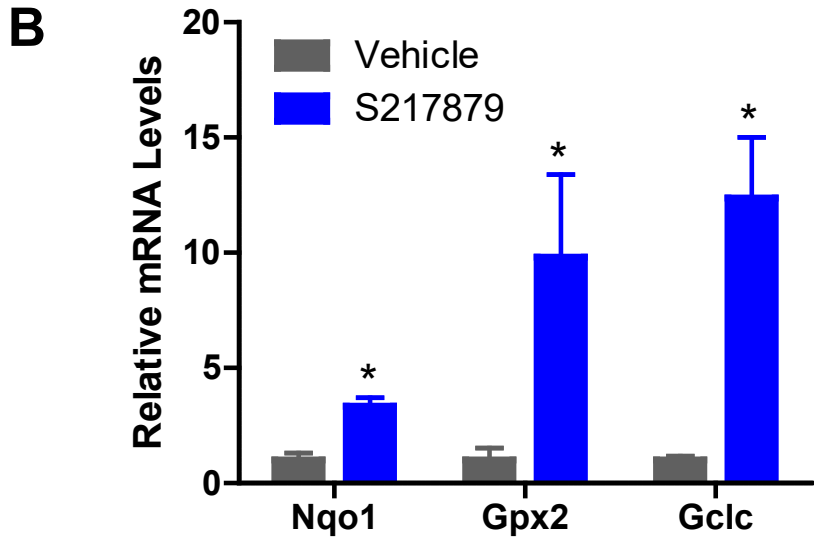

Fig. S2: S217879 treatment leads to reduction in NAS score in MCD-fed mice (A: vehicle; **B:** S218789 3mg/kg; **C:** S217879 30mg/kg). Representative pictures – HE staining.

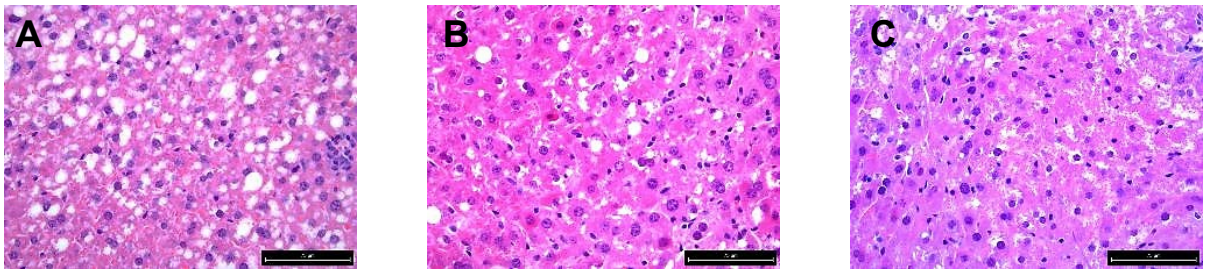

Fig. S3: S217879 treatment leads to reduction in liver triglycerides in MCD-fed mice. Data expressed as mean ± SEM (n=15 per group). Statistical significance was assessed by one-way ANOVA followed by Dunnett's multiple comparison test. (###: p<0.001 A04 vs. MCD vehicle; ***: p<0.001 S217879 vs. MCD vehicle).

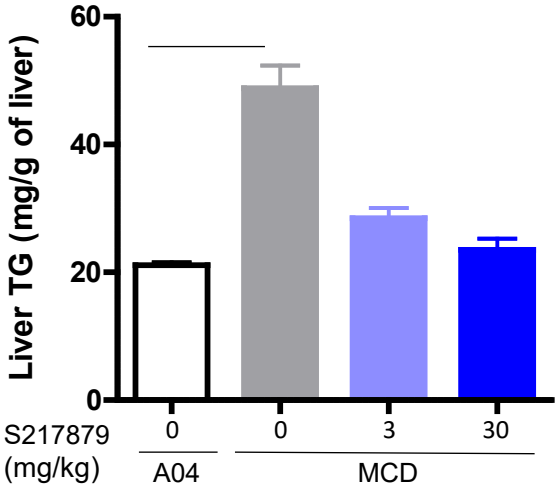

Fig. S4: S217879-mediated NRF2 activation leads to the up-regulation of the antioxidant response and the inhibition of expression of proinflammatory genes in MCD-fed mice. Liver mRNA levels expressed as fold induction over control (A04 fed group) (n=15 per group). Statistical significance was assessed by one-way ANOVA followed by Dunnett's multiple comparison test. ###: p<0.001, ##: p<0.01, #: p<0.05 MCD vs. A04; ***: p<0.001, **: p<0.01 and *: p<0.05 S217879-treated vs. vehicle.

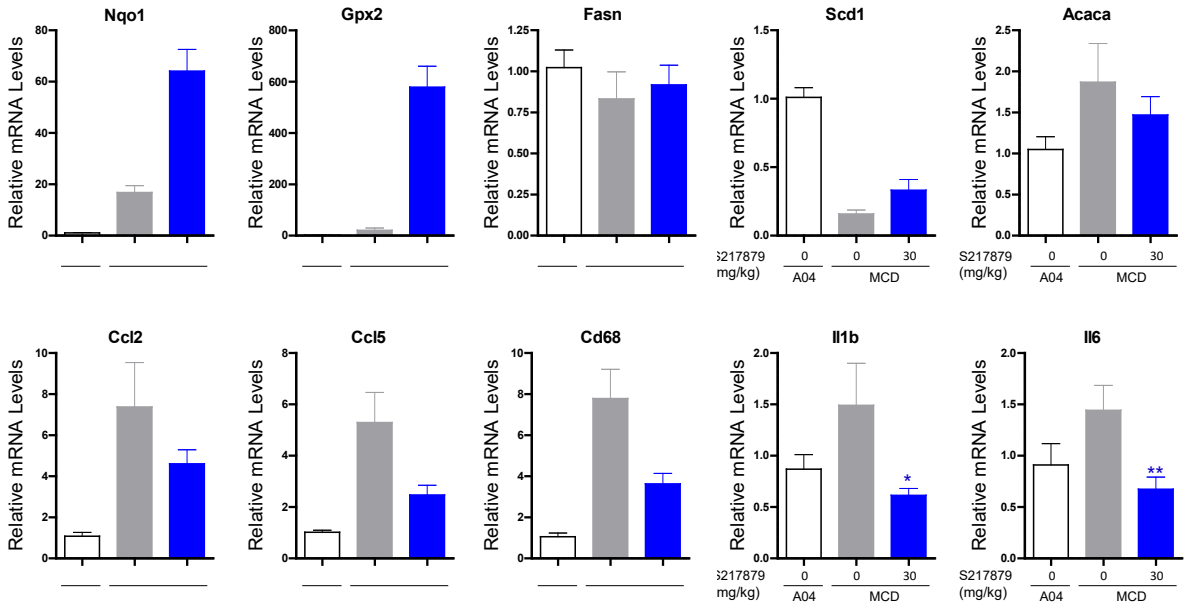

Fig. S5: S217879 treatment leads to reduction in NAS score in MCD-fed mice in a dose-dependent manner. A NAFLD activity scores. **B** Liver Nqo1 mRNA levels expressed as fold induction over control (A04 fed group) (n=15 per group). (***: p<0.001 vs. MCD treated with vehicle).

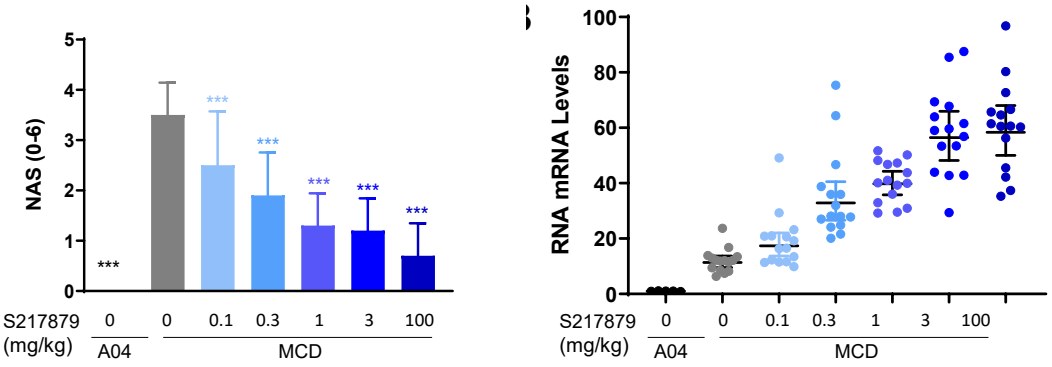

Fig. S6: S217879 treatment did not impact food intake in DIO NASH mice. Food intake expressed as grams per day. Data expressed as Mean ± SEM.

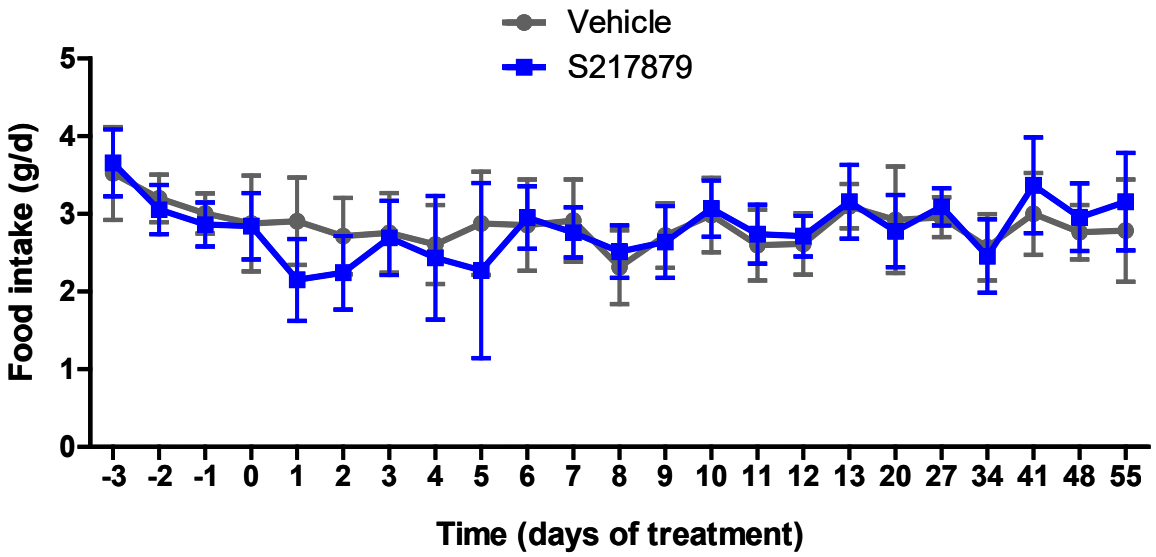

Fig. S7: S217879-mediated NRF2 activation leads to the up-regulation of the antioxidant response and the suppression of a wide spectrum of genes involved in disease progression. Heatmap of core enriched genes derived from GSEA (Differentially Expressed Genes from S217879-treated DIO NASH mice vs. vehicle (Log2 fold change cutoff >1; FDR-adjusted p-value cutoff: 0.05). A: Reactive Oxygen Species, B: Inflammatory response, C: Collagen formation.

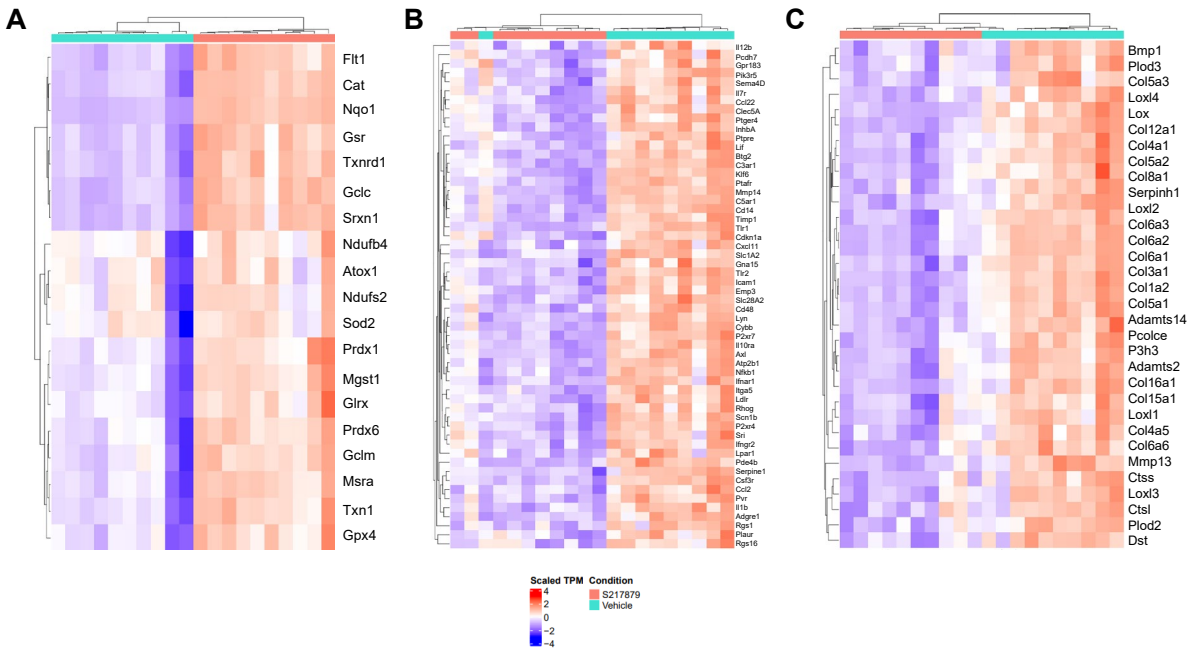

Fig. S8: Expression of differentially expressed genes DIO NASH mice (S217879 30mg/kg vs. vehicle). RNA Seq data are expressed as normalized counts.

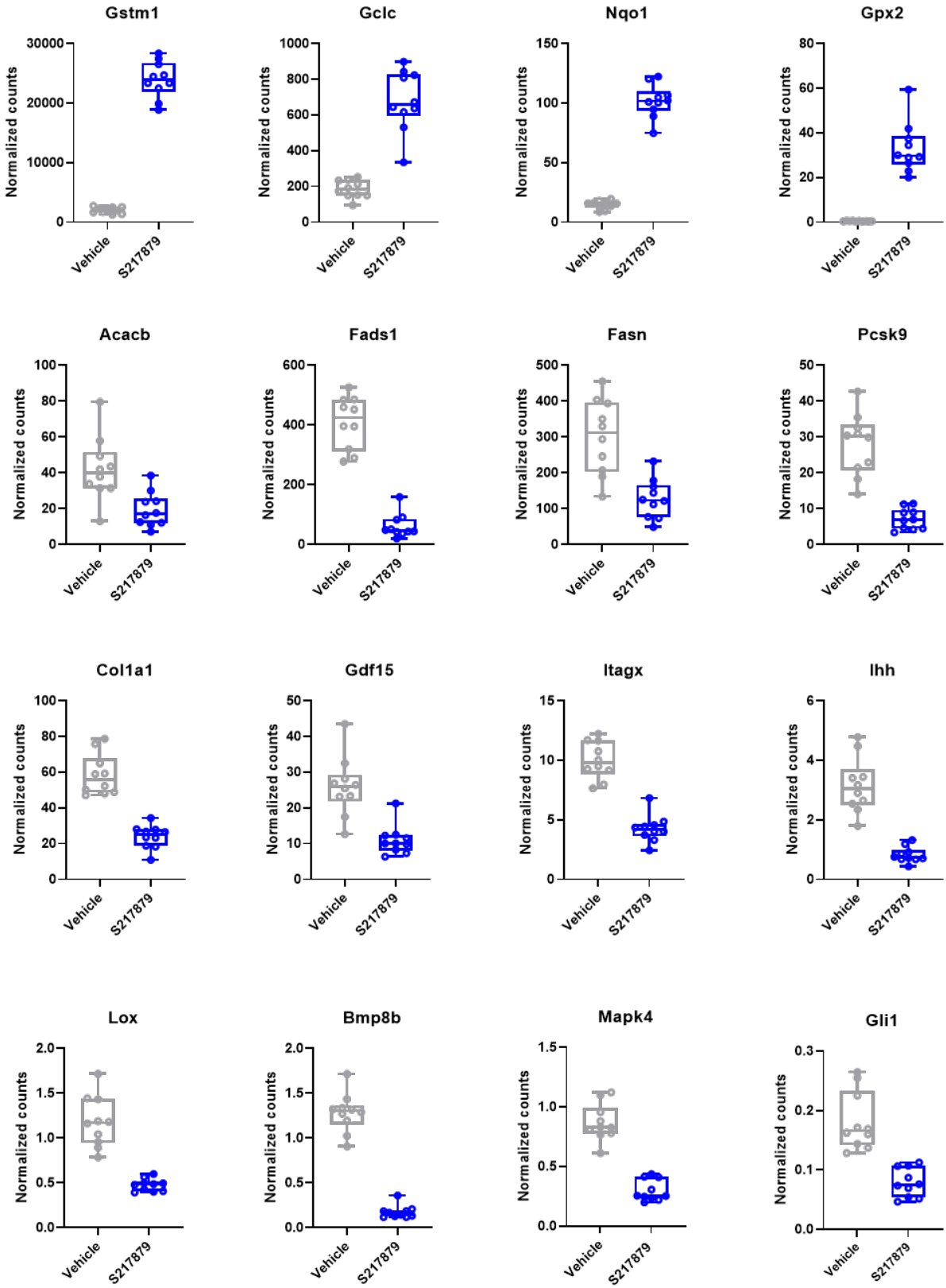

Supplementary tables

Table S1: binding characteristics of S217879 to human KEAP1 (Aa 321-624)

	Kd (M)	K_{off} (s-1)	K_{on} (s-1/M)	Residency time (s)
N=1	3.7 e-9	1.3 e-2	3.6 e+6	76
N=2	4.7 e-9	2.5 e-2	5.4 e+6	40

Table S2: Selectivity data in the CEREP safety panel (S217879 tested at 10µM) – Results expressed as % of inhibition.

Assay	% inhibition	Assay	% inhibition
5-HT (h) (antagonist radioligand)	-4,00	M1 (h) (antagonist radioligand)	-2,00
5-HT1A (h) (agonist radioligand)	-9,00	M2 (h) (antagonist radioligand)	-11,00
5-HT1B (h) (antagonist radioligand)	-11,00	M3 (h) (antagonist radioligand)	5,00
5-HT1D (agonist radioligand)	-12,00	M4 (h) (antagonist radioligand)	1,00
5-HT2A (h) (antagonist radioligand)	-2,00	MT1 (ML1A) (h) (agonist radioligand)	6,00
5-HT2B (h) (agonist radioligand)	-14,00	MT2 (ML1B) (h) (agonist radioligand)	-1,00
5-HT2C (h) (antagonist radioligand)	3,00	mu (MOP) (h) (agonist radioligand)	5,00
5-HT3 (h) (antagonist radioligand)	-17,00	N neuronal alpha 4beta 2 (h) (agonist radioligand)	-6,00
5-HT4e (h) (antagonist radioligand)	-8,00	N neuronal alpha 7 (h) (antagonist radioligand)	-11,00
A1 (h) (antagonist radioligand)	-3,00	Na+ channel (site 2) (antagonist radioligand)	25,00
A2A (h) (agonist radioligand)	-3,00	NK1 (h) (agonist radioligand)	23,00
alpha 1A (h) (antagonist radioligand)	-11,00	NK2 (h) (agonist radioligand)	6,00
alpha 1B (h) (antagonist radioligand)	-11,00	NMDA (antagonist radioligand)	5,00
alpha 1D (h) (antagonist radioligand)	4,00	norepinephrine transporter (h) (antagonist radioligand)	1,00
alpha 2A (h) (antagonist radioligand)	17,00	PPARgamma (h) (agonist radioligand)	4,00
alpha 2B (h) (antagonist radioligand)	-18,00	PR (h) (agonist radioligand)	5,00
alpha 2C (h) (antagonist radioligand)	-4,00	sigma 1 (h) (agonist radioligand)	-2,00
AMPA (agonist radioligand)	2,00	sigma 2 (h) (agonist radioligand)	7,00
AR (h) (agonist radioligand)	11,00	SKCa channel (antagonist radioligand)	0,00
AT1 (h) (antagonist radioligand)	8,00	Y (non-selective) (agonist radioligand)	-20,00
B2 (h) (agonist radioligand)	-3,00	15-Lipoxygenase-2 (h) (recombinant)	26,00
beta 1 (h) (agonist radioligand)	2,00	Abl kinase (h)	20,00
beta 2 (h) (antagonist radioligand)	5,00	ACE (h)	17,00
BZD (central) (agonist radioligand)	-14,00	acetylcholinesterase (h)	13,00
Ca2+ channel (L, dihydropyridine site) (antagonist radioligan	-5,00	adenylyl cyclase (inhibitor effect)	11,00
Ca2+ channel (L, diltiazem site) (benzothiazepines) (antago	17,00	Akt1/PKBalpha (h)	10,00
Ca2+ channel (L, verapamil site) (phenylalkylamine) (antago	1,00	ATPase (Na+/K+)	7,00
CB1 (h) (agonist radioligand)	4,00	CaMK2alpha (h)	6,00
CB2 (h) (agonist radioligand)	8,00	caspase-1 (h)	5,00
CCK1 (CCKA) (h) (agonist radioligand)	-14,00	caspase-3 (h)	5,00
CGRP (h) (agonist radioligand)	0,00	caspase-8 (h)	4,00
choline transporter (CHT1) (h) (antagonist radioligand)	-13,00	CDC2/CDK1 (h) (cycB)	4,00
D1 (h) (antagonist radioligand)	15,00	constitutive NOS (h) (endothelial)	3,00
D2S (h) (antagonist radioligand)	4,00	COX1(h)	3,00
D3 (h) (antagonist radioligand)	4,00	COX2(h)	3,00
D4.4 (h) (antagonist radioligand)	4,00	ECE-1 (h)	3,00
D5 (h) (antagonist radioligand)	3,00	EGFR kinase (h)	2,00
delta (DOP) (h) (agonist radioligand)	11,00	FGFR1 kinase (h)	1,00
dopamine transporter (h) (antagonist radioligand)	28,00	guanylyl cyclase (h) (inhibitor effect)	1,00
Estrogen ER alpha (h) (agonist radioligand)	14,00	inducible NOS	0,00
ETA (h) (agonist radioligand)	0,00	IRK (h) (InsR)	0,00
ETB (h) (agonist radioligand)	-8,00	Lipoxygenase 12-LO	0,00
GABA (non-selective) (agonist radioligand)	-10,00	Lyn A kinase (h)	0,00
H1 (h) (antagonist radioligand)	-31,00	MAO-A (h)	-1,00
H2 (h) (antagonist radioligand)	-26,00	MAO-B (h) recombinant enzyme	-1,00
H3 (h) (agonist radioligand)	-6,00	MEK1/MAP2K1 (h)	-1,00
H4 (h) (agonist radioligand)	-10,00	p38alpha kinase (h)	-1,00
I2 (antagonist radioligand)	-7,00	PDE1B (h)	-3,00
kainate (agonist radioligand)	4,00	PDE2A1 (h)	-4,00
kappa (h) (KOP) (agonist radioligand)	37,00	PDE3A (h)	-4,00
KATP channel (antagonist radioligand)	59,00	PDE4D2 (h)	-5,00
KV channel (antagonist radioligand)	-8,00	PDE5 (h) (non-selective)	-5,00
RAF-1/MEK1 kinase (h)	-17,00	PKA (h)	-8,00
sPLA2 (h) (type V)	-21,00	PKCalpha (h)	-9,00
TRKB (h)	-23,00	PLC	-17,00

Table S3: S217879 ADME-T properties

Parameter	'Species'	Parameter value
Fabs (predicted absorbtion)	Caco-2	97%*
Efflux ratio	Caco-2	4.5**
Solubility	Caco-2	>100 µM
Clint (ml/min/g prot) microsomes / hepatocytes / hepatocytes +plasma	mouse	226 / 340 / 87
	rat	22 / 130 / 58
	dog	122 / 244 / 15
	cyno	243/ 940 / 179
	human	35 / 106 / 21
CYP inhibition (IC50)	human	2C8 ~5 µM, 2C9 ~18 µM
CYP phenotyping	human	>95 % 3A4
hERG inhibition	human	10% @10µM
Nav1.5 inhibition	human	17% @10µM
LD_{50} HepG2 cells	Human	>30µM

* Papp(A to B) = 4.5^{e}-6 cm/s (mass recovery 63%) corresponding to the Fabs=97% value of the table
** Papp(B to A) = 20e-6 cm/s (mass recovery=77%) à efflux ratio = 4.5 (=20/4.5)

Table S4: PK parameters of S217879 at steady state (5 days of administration) in MCD mice (HEC 1% as vehicle)

	3 mg/kg	30 mg/kg
Cmax (µM)	0.3	6.1
AUC (µM.h)	0.62	6.85
Tmax (h)	0.5	0.5

Table S5: S217879 treatment leads to reduction in NAS score in MCD-fed mice.

Steatosis Activity Score

			Difference vs. MCD vehicle		
	Mean	**95% CI**	**Mean**	**95% CI**	**p-value**
Vehicle	2.2	[2.0; 2.4]			
S217879 3mg/kg	1.6	[1.0; 2.1]	-0.6	[-1.2; -0.1]	0.029
S217879 30mg/kg	1	[0.6; 1.4]	-1.2	[-1.7; -0.7]	<0.001

p-value obtained with a statistical model using beta distribution with group as fixed effect on NAS parameter, followed by comparisons of the control and treated groups to the MCD vehicle group. Holm adjustment for multiplicity is applied on the comparison of each dose of S217879 with the MCD vehicle group.

Lobular Inflammation Activity Score

			Difference vs. MCD vehicle		
	Mean	**95% CI**	**Mean**	**95% CI**	**p-value**
Vehicle	1.7	[1.3; 2.0]			
S217879 3mg/kg	1.7	[1.3; 2.0]	0.0	[-0.5; 0.5]	1.000
S217879 30mg/kg	1.2	[0.9; 1.5]	-0.5	[-0.9; 0.0]	0.015

p-value obtained with a statistical model using beta distribution with group as fixed effect on NAS parameter, followed by comparisons of the control and treated groups to the MCD vehicle group. Holm adjustment for multiplicity is applied on the comparison of each dose of S217879 with the MCD vehicle group.

Table S6: S217879 treatment leads to reduction in NAS score in DIO NASH mice.

Steatosis Activity Score – treatment effect

			Difference vs. baseline		
	Mean	**95% CI**	**Mean**	**95% CI**	**p-value**
Vehicle	3	[3.0; 3.0]			
S217879 30mg/kg	2.9	[2.65; 3.07]	-0.04	[-0.32;0.25]	1

Lobular inflammation Activity Score – treatment effect

			Difference vs. baseline		
	Mean	**95% CI**	**Mean**	**95% CI**	**p-value**
Vehicle	2.1	[1.92; 2.23]			
S217879 30mg/kg	1.7	[1.44; 1.98]	-1.41	[-2.06;-0.29]	0.0093

Hepatocellular ballooning – treatment effect

			Difference vs. baseline		
	Mean	**95% CI**	**Mean**	**95% CI**	**p-value**
Vehicle	0.4	[0.13; 0.73]			
S217879 30mg/kg	0.1	[-0.07; 0.35]	-0.12	[-0.52;0.27]	1

Fibrosis stage – treatment effect

			Difference vs. baseline		
	Mean	**95% CI**	**Mean**	**95% CI**	**p-value**
Vehicle	2.4	[2.13; 2.73]			
S217879 30mg/kg	1.8	[1.45; 2.12]	-1.27	[-1.88;-0.66]	0.0003

NAFLD Activity Score – treatment effect

			Difference vs. baseline		
	Mean	**95% CI**	**Mean**	**95% CI**	**p-value**
Vehicle	5.5	[5.2;5.8]			
S217879 30mg/kg	4.7	[4.36; 5.07]	-0.82	[-1.27;-0.38]	0.0008